AGU PUBLICATIONS

Space Weather

RESEARCH ARTICLE
10.1002/2016SW001419

Special Section:
Initial Results from the NASA Radiation Dosimetry Experiment (RaD-X) Balloon Flight Mission

Global real-time dose measurements using the Automated Radiation Measurements for Aerospace Safety (ARMAS) system

W. Kent Tobiska[1], D. Bouwer[1], D. Smart[2], M. Shea[2], J. Bailey[1], L. Didkovsky[1], K. Judge[1], H. Garrett[3], W. Atwell[4], B. Gersey[5], R. Wilkins[5], D. Rice[6], R. Schunk[7], D. Bell[1], C. Mertens[8], X. Xu[8], M. Wiltberger[9], S. Wiley[10], E. Teets[11], B. Jones[12], S. Hong[13], and K. Yoon[13]

[1]Space Environment Technologies, Pacific Palisades, California, USA, [2]Retired, Nashua, New Hampshire, USA, [3]Jet Propulsion Laboratory, California Institute of Technology, Pasadena, California, USA, [4]Space Environment Technologies, Houston, Texas, USA, [5]Department of Electrical Engineering, Prairie View A. & M. University, Prairie View, Texas, USA, [6]Space Environment Corporation, Providence, Utah, USA, [7]Department of Physics, Utah State University, Logan, Utah, USA, [8]NASA Langley Research Center, Hampton, Virginia, USA, [9]National Center for Atmospheric Research, High Altitude Observatory, Boulder, Colorado, USA, [10]Jacobs Technology, Edwards, California, USA, [11]Armstrong Flight Research Center, Edwards, California, USA, [12]Solar Metrics, London, UK, [13]Korea Space Weather Center, JeJu, Korea

Key Points:
- The ARMAS fleet of six instruments can measure the ambient radiation environment at commercial aircraft altitudes at any point on the planet
- Small radiation "clouds" in specific magnetic latitude regions have been identified
- Dose rate doubles every 2 km altitude higher (or halves every 2 km lower), which points to an aviation radiation risk management pathway

Correspondence to:
W. K. Tobiska,
ktobiska@spacenvironment.net

Citation:
Tobiska, W. K., et al. (2016), Global real-time dose measurements using the Automated Radiation Measurements for Aerospace Safety (ARMAS) system, *Space Weather*, *14*, doi:10.1002/2016SW001419.

Received 14 MAY 2016
Accepted 22 OCT 2016
Accepted article online 30 OCT 2016

Abstract The Automated Radiation Measurements for Aerospace Safety (ARMAS) program has successfully deployed a fleet of six instruments measuring the ambient radiation environment at commercial aircraft altitudes. ARMAS transmits real-time data to the ground and provides quality, tissue-relevant ambient dose equivalent rates with 5 min latency for dose rates on 213 flights up to 17.3 km (56,700 ft). We show five cases from different aircraft; the source particles are dominated by galactic cosmic rays but include particle fluxes for minor radiation periods and geomagnetically disturbed conditions. The measurements from 2013 to 2016 do not cover a period of time to quantify galactic cosmic rays' dependence on solar cycle variation and their effect on aviation radiation. However, we report on small radiation "clouds" in specific magnetic latitude regions and note that active geomagnetic, variable space weather conditions may sufficiently modify the magnetospheric magnetic field that can enhance the radiation environment, particularly at high altitudes and middle to high latitudes. When there is no significant space weather, high-latitude flights produce a dose rate analogous to a chest X-ray every 12.5 h, every 25 h for midlatitudes, and every 100 h for equatorial latitudes at typical commercial flight altitudes of 37,000 ft (~11 km). The dose rate doubles every 2 km altitude increase, suggesting a radiation event management strategy for pilots or air traffic control; i.e., where event-driven radiation regions can be identified, they can be treated like volcanic ash clouds to achieve radiation safety goals with slightly lower flight altitudes or more equatorial flight paths.

1. Radiation Sources and Their Effects on Aviation

Aircrew, high-altitude pilots, frequent flyers, and, ultimately, commercial space travelers face galactic cosmic ray (GCR) and solar energetic particle (SEP) radiation hazards (Figure 1), particularly when traveling at and above commercial aviation altitudes, i.e., above 8 km (flight level 260 (FL260) or 26,000 ft). GCRs originate from outside the solar system and consist mostly of energetic protons but also contain heavy ions like iron. SEPs originate from flaring events on the Sun. Regardless of their source, these GCRs, which include p, α, Fe^{+}, and SEPs (mostly protons) penetrate (precipitate) into the Earth's atmosphere. Depending upon their energy, which are sorted by the magnetic field's cutoff rigidity, the charged particles enter the Earth's atmosphere at different magnetic latitudes and impact atmospheric molecules. Below the top of the atmosphere (~100 km), the primary cosmic and solar particles interact with neutral species (predominantly N_2 and O_2) to create secondary and tertiary particles and photons, such as n, p, e, α, π, μ, and γ rays. These primary particle fluxes decrease with decreasing altitude due to absorption by atmospheric molecules, while the secondary radiation component from lower energy cascading particles and photons created by those impacts increases. These competing processes (decreasing primaries and increasing secondaries with lower altitudes) produce a maximum ionization rate that occurs between 20 and 25 km (65,000–82,000 ft) and is called the Pfotzer maximum. Below this altitude, down to the Earth's surface, the dose rate then decreases with particle or

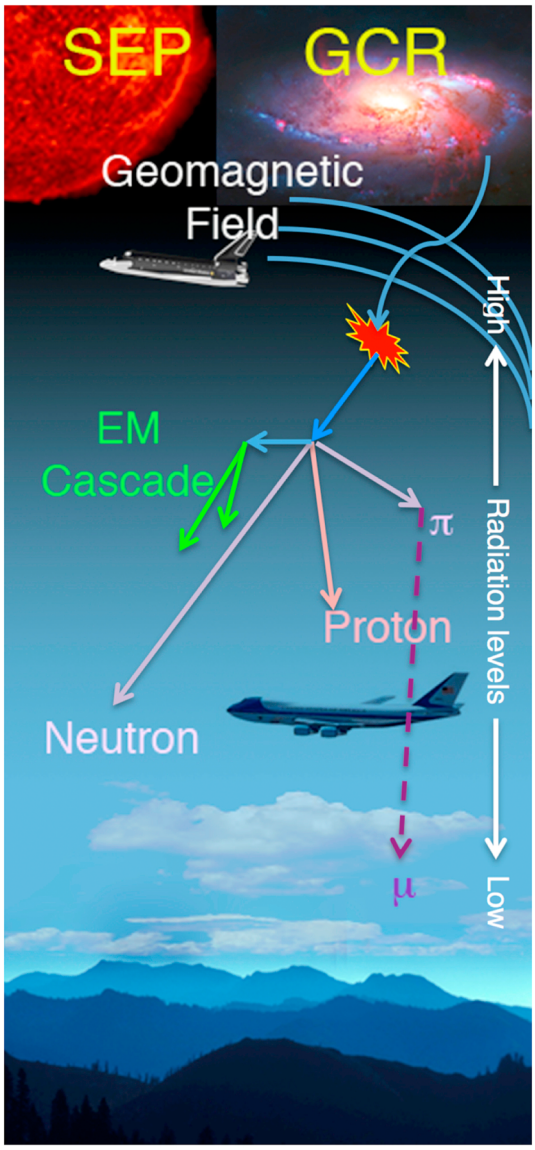

Figure 1. The complex radiation environment at and above commercial aviation altitudes due to GCRs and SEPs [*Tobiska et al.*, 2015].

photon absorption in an increasingly thick atmosphere. The broad spectrum of secondary particles consists of varying energies with neutrons and protons that can radiate in all directions but are generally directed downward. Those secondary and tertiary particles collide with an aircraft hull and interior components, people, or fuel to cause a further alteration of the radiation spectrum.

This complex radiation field has components, including neutrons, which have been shown to cause an increased cancer risk and are of special interest to the cancer research community. Atmospheric ionizing radiation is the primary source of human exposure to high linear energy transfer (LET) radiation at commercial aircraft altitudes [*Wilson et al.*, 1995; *European Commission Radiation Protection 140*, 2004; *Jones et al.*, 2005; *Mertens et al.*, 2010]. High LET radiation is effective at directly breaking DNA, which can lead to cancer or other adverse health effects that can limit careers of aircrew, for example [*Cannon*, 2013]. Several mechanisms can cause injury to living tissue when this radiation causes atoms and molecules to become ionized, dissociated, or excited. These include (i) production of free radicals, (ii) breakage of chemical bonds, (iii) production of new chemical bonds and cross-linkage between macromolecules, and (iv) damage of molecules that regulate vital cell processes, e.g., deoxyribonucleic acid (DNA), ribonucleic acid (RNA), and proteins. Although cells can repair certain levels of damage from low doses, such as those received daily from ambient radiation near the surface of the Earth, cell death is the most likely result from higher doses. At extremely high doses, cells cannot be replaced quickly enough and the tissue fails to function normally [*International Agency for Research on Cancer*, 2000; *United Nations Scientific Committee on the Effect of Atomic Radiation*, 2000].

2. Radiation Specification at Aircraft Altitudes

The White House-directed Space Weather Strategy and Action Plan (SWAP) [*National Science and Technology Council*, 2015] and Executive Order Coordinating Efforts to Prepare the Nation for Space Weather Events [*Executive Order 13744*, 2016] support the development and validation of an operational radiation monitoring and forecasting capability. In particular, SWAP seeks to (i) define the requirements for real-time monitoring of the charged particle radiation environment to protect the health and safety of crew and passengers during space weather events; (ii) define the scope and requirements for a real-time reporting system that conveys situational awareness of the radiation environment to orbital, suborbital, and commercial aviation users

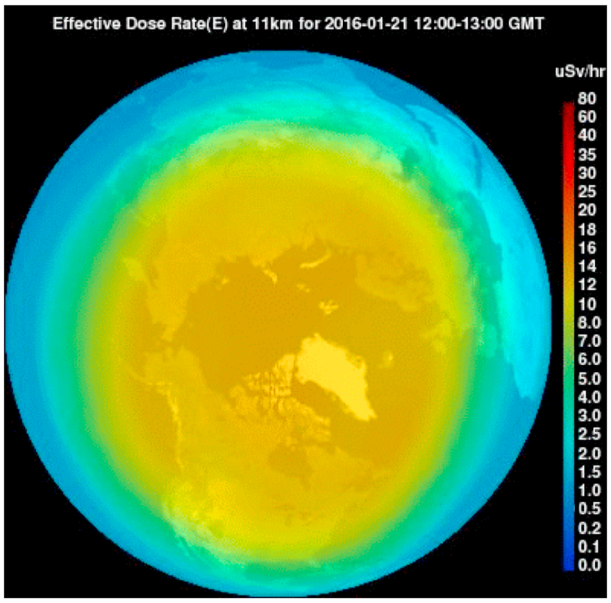

Figure 2. The NAIRAS Northern Hemisphere hourly effective dose rate at 11 km.

during space weather events; and (iii) develop or improve models for the real-time assessment of radiation levels at commercial flight altitudes. The Automated Radiation Measurements for Aerospace Safety (ARMAS) program directly supports the measurement (monitoring), reporting (situation awareness), and modeling (specification and forecasting) thrusts of the SWAP and Executive Order (EO) 13744 initiatives.

2.1. Status of Measurements

Until recently, the method of measuring dose at aviation altitudes was by in situ instruments that were returned after flight for analysis. This method has provided a wealth of data related to the aviation radiation environment and has made important contributions to model validations of the radiation field at altitude, especially for human tissue damage. A large number of measurements used for postflight analysis have been made using Tissue Equivalent Proportional Counters (TEPCs) under GCR background conditions and not during major space weather SEP events [*Dyer et al*., 1990; *Beck et al*., 1999; *Kyllönen et al*., 2001; *European Commission Radiation Protection 140*, 2004; *Getley et al*., 2005; *Beck et al*., 2005; *Latocha et al*., 2007; *Meier et al*., 2009; *Beck et al*., 2009; *Dyer et al*., 2009; *Hands and Dyer*, 2009; *Getley et al*., 2010; *Gersey et al*., 2012; *Tobiska et al*., 2014a, 2014b, 2015]. Some of the measurements have included neutron flux and dose equivalent measurements with solid-state detectors [*Dyer et al*., 2009; *Hands and Dyer*, 2009; *Ploc et al*., 2013; *Lee et al*., 2015].

To date, however, the difficult task of continuous radiation environment monitoring, reporting, and modeling has not yet been achieved. Specifically, there are few global, routine, real-time, and validated ambient dose equivalent (tissue) or absorbed dose (silicon) measurements. Because monitoring in particular does not exist, and because very few in-flight radiation measurements during significant solar particle events have occurred, it remains an important task to fly calibrated instruments as widely and often as possible to maximize the data volume that can both validate models and potentially assist in creating data-assimilated "weather" of the radiation environment, similar to what has occurred in the tropospheric weather community during the past few decades. The ARMAS program has undertaken the task of developing a calibrated, real-time, global monitoring, reporting, and modeling capability.

2.2. Status of Operational Modeling

There are five altitude domains (deep space, low Earth orbit (LEO), suborbital, high altitude, and commercial aviation) in which radiation affects human activity, and they need to be considered as a whole system. In this paper we exclude deep space missions (beyond LEO to the Moon and Mars) due to the scope of required work. In the near term, as human activity to space becomes more common, there is a stated need (SWAP and EO 13744) to operationally and self-consistently specify and forecast the radiation environment from the ground to LEO in real time. Fulfilling this critical need will help ensure human and avionics flight safety.

The early stages of this capability are now being constructed. One example of the current state-of-the-art core for an operational system is NASA Langley Research Center's (LaRC) *Nowcast of Atmospheric Ionizing Radiation for Aviation Safety* (NAIRAS) system [*Mertens et al*., 2012, 2013]. NAIRAS is a data-driven, physics-based climatological model (Figure 2) producing time-averaged weather conditions using the ISS HZETRN radiation transport code that characterizes the global radiation environment from the surface to LEO for radiation dose rate and total dose hazards. Global, data-driven results are reported hourly at http://sol.spaceenvironment.net/~nairas/index.html. However, to produce the weather of the radiation environment, NAIRAS

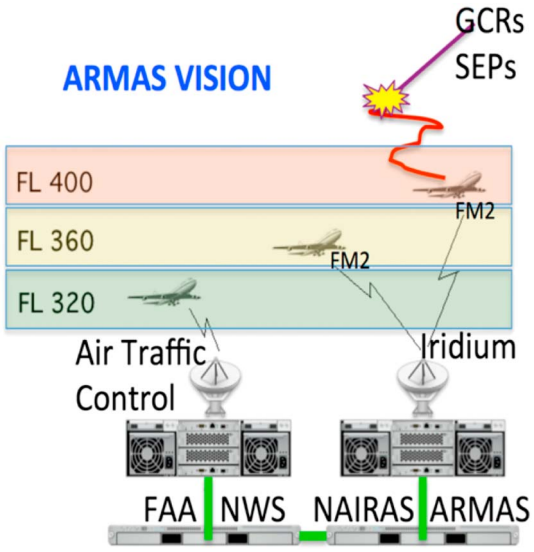

Figure 3. ARMAS program vision that integrates real-time dose rate measurement technologies into operational aerospace and space traffic management systems.

needs assimilated real-time data. Consider the analogy of tropospheric weather models that need temperature, pressure, and species' concentrations to make accurate weather reports. Similarly, for specifying radiation weather, models need data at recent epochs and global locations. NAIRAS input data for assimilation will consist mostly of total ionizing dose (TID), either as an absorbed dose or ambient dose equivalent although other, more complex measurements can be included where available.

The ARMAS program, developed by Space Environment Technologies (SET) through a NASA Small Business Innovation Research (SBIR) project, is now creating these TID data. For data assimilation into operational NAIRAS [*Tobiska et al*., 2015], TID can be used as a low-cost index to express the context of full energy spectrum measurements. The latter are ideal but often not feasible due to instrument size, mass, and data volume considerations. TID is analogous to total electron content (TEC) used in ionospheric data assimilation models. ARMAS uses a TID commercial-off-the-shelf (COTS) micro dosimeter combined with a microprocessor and electronics package plus a variety of real-time data collection methods (Iridium, Bluetooth, RS232, Ethernet, or micro-SD cards) to report the dose rate from aircraft during flight. This technology readiness level (TRL) 8 system as shown in Figure 3 has been flying on research and commercial aircraft starting in 2013. Aircraft platforms include the NASA Armstrong Flight Research Center's (AFRC) DC-8, B-747, and ER-2 as well as the NOAA and NSF/NCAR (National Center for Atmospheric Research) G-IV and G-V Gulfstreams, respectively. ARMAS units have also flown on Boeing 737, 747, 757, and 777 as well as Airbus 319 and 320 commercial jets; ARMAS has also flown on lower altitude aircraft such as the Bombardier Q200. The maximum altitude covered by all aircraft is FL560 on the ER2, i.e., below the 20 km Pfotzer maximum.

2.3. The ARMAS Program

Evolving from NASA SBIR Phases I–III, ARMAS has the goal of building, demonstrating, and deploying a system that not only includes a fleet of radiation measurement flight units making real-time dose measurements but is able to retrieve those data and immediately process them into tissue-relevant units for use by end users. Having a fleet of instruments that can operationally monitor radiation in aircraft, balloons, rockets, reusable launch vehicles, and satellites would enable real-time identification of radiation hazards during space weather events, including those with solar protons and geomagnetically disturbed conditions.

ARMAS has already obtained real-time radiation measurements from the ground to 17 km through 213 flights. The altitude regime from 17 to 40 km is ideal for making balloon measurements and, to measure the regime above 40 km, it requires sounding rockets, reusable launch vehicles, or cubesats. The altitude regime around 20–25 km encompasses the Pfotzer maximum, and measurements below, through, and above this region are sparse but particularly useful for understanding the complex transformation of the primary radiation particle and energy spectrum as charged particles strike atmospheric species. The RaD-X project [*Mertens et al*., 2016] has contributed to this knowledge. All these types of measurements can help near-term validation of systems like NAIRAS as well as provide potential data assimilation capabilities for physics-based models. However, understanding the effect of space weather (solar wind high-speed streams, coronal mass ejections, enhanced proton flux events, and other disturbances to the magnetospheric magnetic field) is an area of continuing, necessary research. In particular, the variation in cutoff rigidities, which act as "gatekeepers" by allowing greater or lesser numbers of protons or other charged particles of a given

Table 1. ARMAS Phase I TEPC Flight Dosimetry Result Summary

	Flight Origin (2011)		Flight Destination		Dose[a]	Rate[b]	Dose[c]	Rate[d]	Q^e
#	UT Date[f]	Site	UT Date	Site	(μGy)	(μGy h^{-1})	(μSv)	(μSv h^{-1})	Q
1	04/28 12:26:00	Holbrook, NY	04/28 14:43:00	Memphis, TN	2.34	1.28	5.88	3.29	2.55
2	06/16 1:56:00	Holbrook, NY	06/16 3:40:00	Indianapolis, IN	1.19	1.17	2.63	2.70	2.24
3	08/25 7:06:00	Houston, TX	08/25 10:07:00	Los Angeles, CA	2.20	1.03	3.96	1.81	1.72

[a]Total absorbed dose.
[b]Absorbed dose rate.
[c]Total dose equivalent.
[d]Total dose equivalent rate.
[e]Average quality factor.
[f]Dates are formatted as month/day.

energy to enter the lower atmosphere along specific magnetic latitudes (L shells), is an active area of study as is how energetic electron precipitation from the outer radiation belt affects the atmospheric radiation environment. The ARMAS measurements, described below, provide data to assist these efforts.

2.3.1. Purpose

The ARMAS program vision (Figure 3) is designed to monitor, report, and model in real time the atmospheric radiation environment and provide an actionable information flow to two commercial aviation needs for aiding human tissue radiation risk management: knowledge of the state of long-term background radiation from GCR sources that can impact crew monthly, annual, and career statistical dose limits; and identification of short-term hazards from space weather events that could lead to increased deterministic risk for radiation illness.

With this purpose in mind, ARMAS has proceeded through NASA SBIR Phases I, II, IIE, and III to achieve several important TRL milestones:

1. 2010 (TRL 5) created a global physics-based radiation climatology real-time data stream as input into NAIRAS prototype operations (NAIRAS DECISION).
2. 2011 (TRL 5) performed in situ dose rate measurements on commercial aircraft (ARMAS Phase I).
3. 2013 (TRL 5) calibrated TID measurements with tissue-relevant data using national beam line facilities (ARMAS Phase II).
4. 2013 (TRL 6) retrieved the first autonomous, real-time measurements from commercial altitudes with 15 min latency (ARMAS Phase II).
5. 2015 (TRL 7) demonstrated system-level processing in a relevant operational environment with three ARMAS units operating simultaneously in Northern and Southern Hemispheres (ARMAS Phase IIE).
6. 2016 (TRL 7) obtained global dose rate data records from 213 flights.
7. 2016 (TRL 8) released real-time ARMAS weather and NAIRAS climatology ambient dose rate equivalent comparison with a 5 min latency from locations around the Earth (ARMAS Phase III).

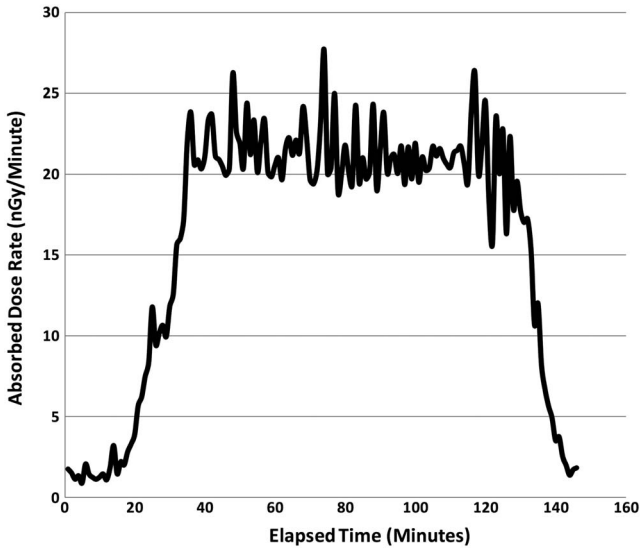

Figure 4. TEPC flight 1 absorbed dose rate from Holbrook, New York, to Memphis, Tennessee, on 28 April 2011.

2.4. ARMAS SBIR Phase I

The Phase I ARMAS project evolved from the successful NAIRAS project [*Mertens et al.*, 2013] when a dose rate data source need was recognized.

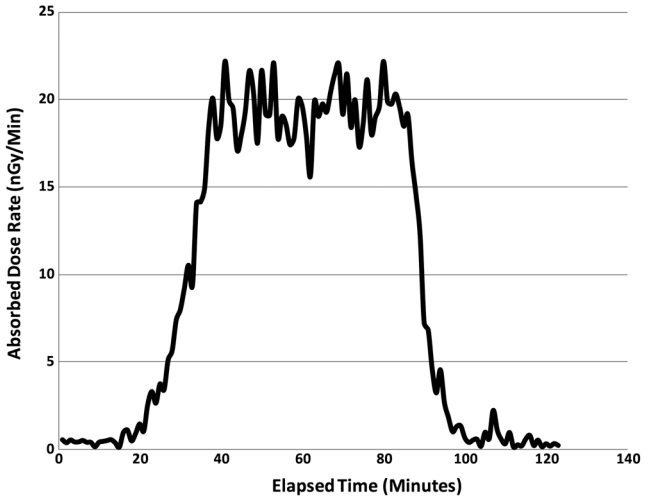

Figure 5. TEPC flight 2 absorbed dose rate from Holbrook, New York, to Indianapolis, Indiana, on 16 June 2011.

Phase I activities verified that ambient dose equivalent measurements could be made at commercial altitudes consistent with NAIRAS modeling. In section 2.1, we identified a number of teams that have previously accomplished similar data-gathering tasks, but we had to demonstrate that our team could also accomplish this data collection and postanalysis work. Prairie View A. & M. University (PVAMU), as part of our team, deployed and obtained data from a TEPC, aka "Hawk," dosimeter. It was sealed in a steel container and flown successfully on three commercial cargo flights as described below and in Table 1.

TEPC Flight 1 from Holbrook, New York (12:26:00 UT), to Memphis, Tennessee (14:43:00 UT), on 28 April 2011 had a total absorbed dose of 2.34 μGy, an absorbed dose rate of 1.28 μGy h^{-1} at an estimated 9.8 km cruise altitude, a total dose equivalent of 5.88 μSv, and a total dose equivalent rate of 3.29 μSv h^{-1}. Figure 4 shows the measured absorbed dose rate (μGy h^{-1}) as a function of elapsed time in minutes.

TEPC Flight 2 from Holbrook, New York (01:56:00 UT), to Indianapolis, Indiana (03:40:00 UT), on 16 June 2011 had a total absorbed dose of 1.19 μGy, an absorbed dose rate of 1.17 μGy h^{-1} at an estimated 9.8 km cruise altitude, a total dose equivalent of 2.63 μSv, and a total dose equivalent rate of 2.70 μSv h^{-1}. Figure 5 shows the measured absorbed dose rate (μGy h^{-1}) as a function of elapsed time in minutes.

TEPC Flight 3 from Houston, Texas (07:06:00 UT), to Los Angeles, California (10:07:00 UT), on 25 August 2011 had a total absorbed dose of 2.20 μGy, an absorbed dose rate of 1.03 μGy h^{-1} at an estimated 9.8 km cruise altitude, a total dose equivalent of 3.96 μSv, and a total dose equivalent rate of 1.81 μSv h^{-1}. Figure 6 shows the measured absorbed dose rate (μGy h^{-1}) as a function of elapsed time in minutes.

In Phase I, we made a high-level comparison between the 2011 dose equivalent rate (μSv h^{-1}) ARMAS Phase I TEPC flights 1, 2, and 3 at 9.8 km with then-available NAIRAS 5, 11, and 15 km CONUS midlatitude data sets (Figure 7). NAIRAS 1σ error bars are shown (2011 NAIRAS version—blue) as well as a 13–14 February 2008 Deutsches Zentrum für Luft- und Raumfahrt (DLR) TEPC flight at 11 km from Düsseldorf, Germany (DUS), to Port Louis, Mauritius (MRU), across magnetic equatorial Africa [*Hubiak*, 2008] (gray). We also include two ranges of variation for ARMAS flights, one (A1—orange) between Los Angeles, California, and New Orleans, Louisiana, that is comparable with the TEPC 3 data point (Houston, Texas, to Los Angeles, California) and a second (A2—orange) Case 4 discussed below for a typical CONUS midlatitude flight between Los Angeles, California, and Washington, District of Columbia.

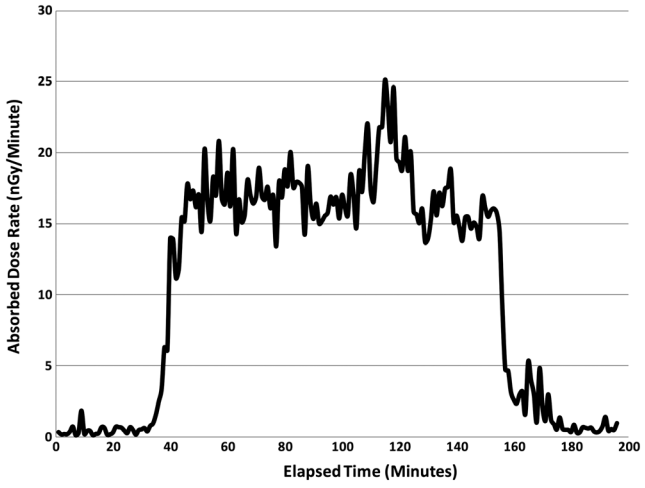

Figure 6. TEPC flight 3 absorbed dose rate from Houston, Texas, to Los Angeles, California, on 25 August 2011.

This comparison verified a reasonable, order-of-magnitude match between ARMAS Phase I data and

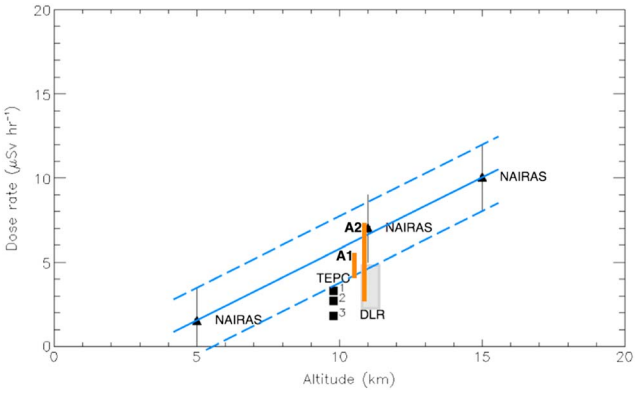

Figure 7. Dose rate comparison for NAIRAS (triangles), ARMAS TEPC (squares), ARMAS FM (orange bars), and DUS-MRU TEPC (gray rectangle).

models. Though the NAIRAS data in Figure 7 appears to overpredict the dose rate for this altitude regime, this comparison should only be used for an order-of-magnitude estimate. In this figure, we used generic NAIRAS midlatitude runs for these altitudes and did not incorporate the actual space weather-driven conditions, including the environment from GCRs during those dates or magnetic latitudes that could change the NAIRAS results. In addition, from RaD-X results, it was found that TEPC tends to underpredict the absorbed dose rate of a reference low LET radiation source by 16%. This would increase the TEPC 1, 2, and 3 values.

2.5. ARMAS SBIR Phases II, IIE, and III

In Phases II, IIE, and III the ARMAS team made TID and TEPC calibration measurements at national laboratories, retrieved autonomous real-time dose measurements from aircraft, brought the data to the ground for low-latency processing, and then made automated comparison of it with NAIRAS current epoch data cube. This technology demonstration showed how a data stream could be created to help validate NAIRAS and then be used as a future data source for assimilation so as to specify global radiation weather. We also retrieved simultaneously, for the first time, real-time measurements from three separate aircraft flying in the Northern and Southern Hemispheres during October 2015. By October 2016 we had flown 213 global flights providing 120,446 data records. Our success at demonstrating a TRL 8 system for calibrated, global ambient dose equivalent rate data in real time is described below using five cases.

The measurements from aircraft were made in real time with ARMAS Flight Module (FM) instruments that are described next. These FMs demonstrated a capability of (i) flying dosimeters on aircraft, (ii) making measurements of the absorbed dose in silicon, (iii) collecting the measurements in an automated method, (iv) transmitting them to the ground; (v) retrieving the downlinked Level 0 raw total dose increments (mV), (vi) processing them through Level 3 ambient dose equivalent rates ($\mu Sv\,h^{-1}$), (vii) comparing the Level 3 data to the NAIRAS hourly values at that location, and (viii) reporting the radiation information to agency, commercial, and public users. Our near-term goal is to improve aviation safety by characterizing the weather of the radiation environment, i.e., its state at a particular time and place (cf. *Merriam-Webster Dictionary*), compared to its climatological or time-averaged weather conditions along a flight track (cf. National Weather Service Climate Prediction Center Climate Glossary). We consider that NAIRAS produces data-driven climatological information, using inputs such as neutron monitor counts, GOES particle fluxes, NCEP 3 h global reanalysis data, SEPs, and other data to create a physics-modeled environment. We note from the ARMAS and NAIRAS comparison that the particular time and place features in the NAIRAS data are not represented but the averaged conditions are instead produced. The ARMAS system latency is 5 to 15 min, depending upon the particular flight instrument that is used.

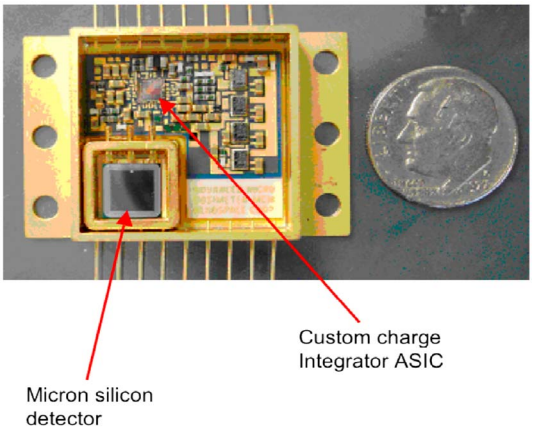

Figure 8. Teledyne micro dosimeter chip used in ARMAS.

2.6. Use of Teledyne Micro dosimeters

The SET ARMAS instruments use Teledyne micro dosimeters (UDOS001, Figure 8), which directly measure TID absorbed by an internal silicon test mass. The detector size is $3.56 \times 2.54 \times 0.10$ cm. By accurately measuring the energy absorbed from electrons, protons, neutrons, and gamma rays, an estimate of the absorbed dose in silicon can be made. The micro dosimeter can operate from a wide range of input power voltages that are >13 V. The accumulated dose is reported via three DC linear and one pseudologarithmic outputs in units of millivolts, giving a dose resolution of 14 μrads and a measurement range exceeding 100 krads. This micro dosimeter is the first compact microcircuit that provides a repeatable measurement of radiation total absorbed dose in silicon (TID) over a wide range of energies (60 keV to 15 MeV) and operating temperatures (−30 to +40°C). Temperature effects can be a consideration for the micro dosimeter results, and, to obtain the best accuracy for low dose rates, operation at or below 25°C is recommended by Teledyne. In ARMAS, the instrument is typically operated at aircraft cabin temperatures (15–25°C), although colder temperatures to −30°C can be experienced in the ER-2 Q-bay instrument rack, i.e., the lower operating limit of the device. Developed by Aerospace Corporation and manufactured under license by Teledyne, the UDOS001 micro dosimeter produces a flat energy response, has high reliability, and can be tested without a radiation source. It is currently being flown on the Lunar Reconnaissance Orbiter (LRO) and DoD satellites as well as by ARMAS.

3. ARMAS Flight Modules

The ARMAS Flight Module (FM) is a system with two components: (i) a flight instrument that can measure the real-time radiation environment TID on an aircraft and (ii) a calibrated data stream from the aircraft to the ground, then processed to Level 3 geophysically relevant data. Measurements are made using the Teledyne micro dosimeter UDOS001 (μDos) in combination with a microprocessor, a GPS chip, an Iridium transceiver, a Bluetooth antenna, a data logger using a micro-SD card, and associated electronics. All these are mated to a printed circuit board and housed in either a milled aluminum or 3-D printed nylon case. Once the absorbed dose (Si) is measured within the aircraft, it is relayed via an active Iridium satellite link to the ground or Bluetooth/WiFi to a computer/app on board. Four generations of FMs are shown in Figure 9, each with a smaller form factor and added capabilities compared to the previous generation.

3.1. Flight Instruments

First, Flight Module 1 (FM1—Figure 9a) is the original unit that was developed as the Phase II prototype demonstration for use on the NASA AFRC DC-8. Delivered in May 2013, it consists of three electronics boxes fit onto a 60.96×91.44 cm aluminum rack mount plate with a mass of 15.60 kg. The ARMAS dosimeter (blue box), Atmospheric and Space Technology Research Associates (ASTRA) CASES GPS (black box), and system communications electronics (silver box with NASA logo) are externally powered with aircraft 60 Hz 110VAC. FM1 produces 1 min data records of time, latitude, longitude, altitude, and dose, sending it down every 5 min in an Iridium Short Burst Data (SBD) burst. Second, there are two nearly identical FM2 units (Figure 9 b) that are enclosed in milled aluminum cases for the NOAA Gulfstream IV (FM2A delivered February 2015) and the NSF/NCAR Gulfstream V (FM2B delivered March 2015). These were built with financial assistance from, and are now owned by, the South Korean Space Weather Center. They are externally powered using aircraft 60 Hz 110VAC and have dimensions of $14.73 \times 18.80 \times 4.06$ cm with a mass of 0.45 kg. They provide the same data records, with the same cadence, as FM1 via Iridium real-time downlinks. Third, the FM3 unit is in an enclosed milled aluminum case and was built for the NASA AFRC ER-2, delivered May 2015. It has dimensions of $16.00 \times 18.29 \times 4.32$ cm with a mass of 0.50 kg (Figure 9c). Externally powered with aircraft 28 Volts DC, the 10 s data is sent through the aircraft Ethernet (NASDAT) datalink or can be stored on a micro-SD card data logger. Fourth, the two identical FM5 prototype carry-on commercial units (Figure 9d) were delivered April 2016, one to NASA AFRC (FM5A), and are enclosed in a 3-D printed nylon box with dimensions of $9.14 \times 14.99 \times 3.81$ cm and a mass of 0.50 kg. In addition to Iridium, GPS, and Bluetooth connections, there is a micro-SD card data logger for the 10 s data; an internal, rechargeable Li^+ polymer 10,000 mAh battery powers FM5.

3.2. Calibrated Data Stream

This fleet of six ARMAS FM instruments has produced Level 2 absorbed dose rates in silicon and Level 3 ambient dose equivalent rates for 213 flights since 2013. The Level 0 data are sampled at 10 s (0.1 Hz) or 1 min (0.0167 Hz), and the four-channel voltages are multiplied by 1000 for transmitted bit reduction prior to

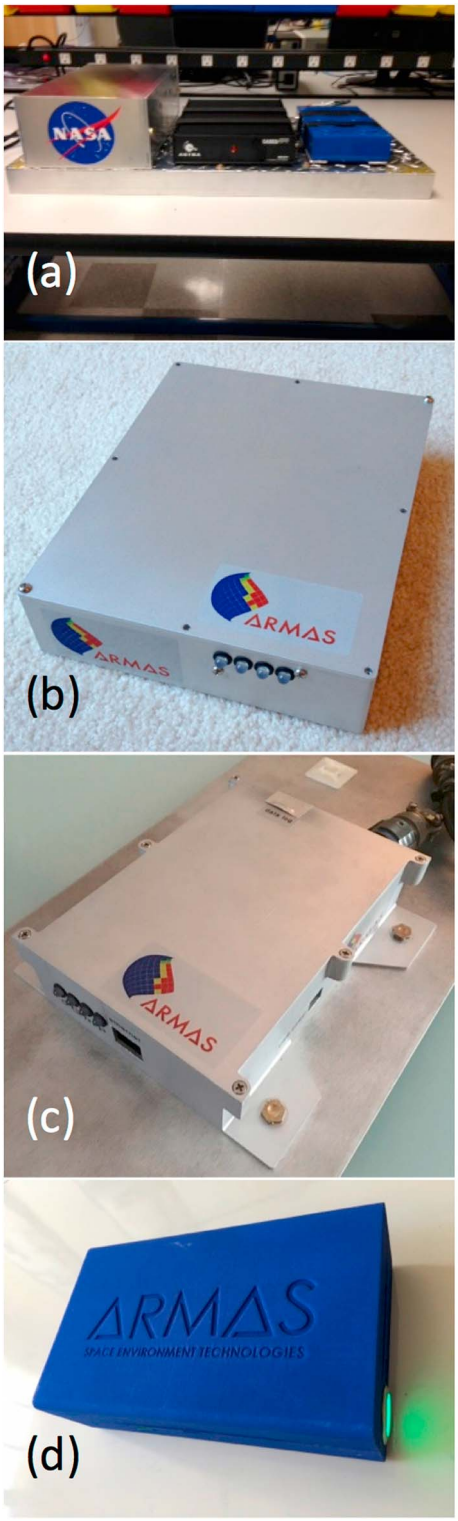

Figure 9. (a) ARMAS FM1 for the DC-8, (b) FM2 for the NOAA G-IV and NSF/NCAR G-V, (c) FM3 for the NASA AFRC ER-2, and (d) FM5 carry-on for NASA and commercial aircraft.

placing in the data packets. The data packets are then downlinked every 50 s or 5 min, respectively, via Iridium short data bursts, as well as optionally sent via Bluetooth to onboard computers/apps and logged to the micro-SD card, depending on the unit. The detector can sample up to 50 Hz, but due to operational constraints (Iridium SBD costs) the instruments are operated at a lower sample rate. This is an advantage in atmospheric radiation monitoring since it allows for accumulated dose integration that aids in statistical noise reduction in the measured signal. Once received on the ground, the Level 0 raw data of UT time, latitude, longitude, and engineering unit (mV) accumulated dose are immediately processed to Level 1 total dose (rad) using the Teledyne recommended voltage-to-dose conversion method [*Mazur et al.*, 2011], where channels 1–3 (already having been multiplied by 1000 in the Level 0 transmitted packets) are then converted to total absorbed dose or total ionizing dose, TID. We calculate TID = ch1*14.0E−2 + ch2*3.6E+1 + ch3*0.9E+4 μGy at Level 1. The Level 2 absorbed dose rates in silicon ($\mu Gy\,h^{-1}$) are then created by calculating the numerical difference of the current time record TID over the previous 20 measurement time steps and then converting to 1 h time intervals. The Level 3 ambient dose equivalent rate in tissue ($\mu Sv\,h^{-1}$) data are then created by multiplying the Level 2 total absorbed dose rate in Si by a conversion factor between Si and Ti, by a normalized ambient dose equivalent factor for the GCRs and SEPs, by an instrument correction absorbed dose calibration factor, and by the cutoff rigidity-dependent quality factor. The processed Levels 2 and 3 data are subsequently released at the http://sol.spaceenvironment.net/~ARMAS/index.html website with latencies from the time of measurement on the plane to the user of between 5 and 15 min. Level 2 and 3 data are compared with the most recent hour's NAIRAS global radiation climatological model

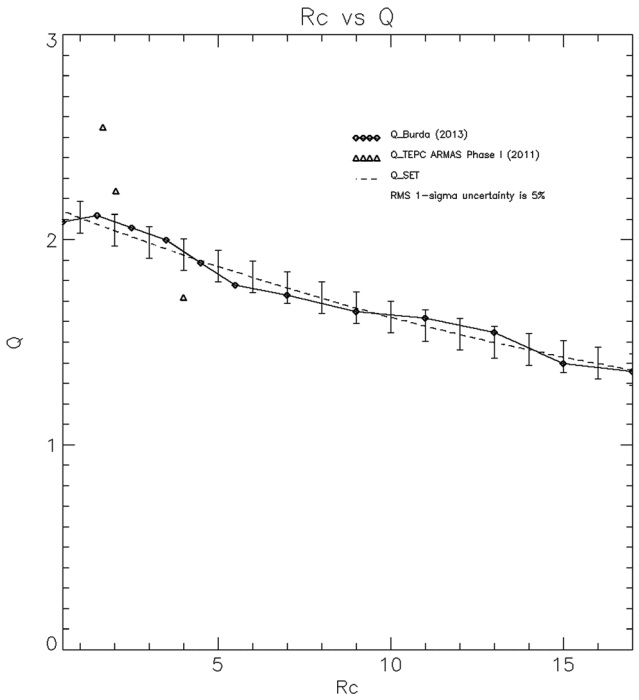

Figure 10. Quality factor calculation as a function of vertical cutoff rigidity, Rc.

output (http://sol.spacenvironment.net/~nairas/index.html) with the results presented both visually through jpeg plots and through text files. For this paper we have adopted the *Mertens et al*. [2016] NAIRAS uncertainty with prior aircraft measurements of 10% at high latitudes and low cutoff rigidities, increasing to 50% for low latitudes and high cutoff rigidities. For figures in this paper with ARMAS and NAIRAS comparison, we apply an analytic function to scale the NAIRAS 1 sigma error bars between 10 and 50% based on the Rc of the aircraft position.

In *Mertens et al*. [2016] and *Straume et al*. [2016] the TID is considered sensitive to energies between 0.1 and 15 MeV with lineal energy deposition from 0.4 to 60.0 keV μm^{-1}. This is also consistent with *Mazur et al*. [2011] who were instrumental in originally developing the detector. However, their previous work had not yet been able to quantify the TID detector response in a neutron beam environment; the energy spectrum of atmospheric neutrons extends from 1 to 800 MeV [*Gersey et al*., 2003].

In work still being analyzed, our team performed laboratory comparisons between the TEPC and the Teledyne instruments in the Los Alamos Neutron Science Center (LANSCE) 30L neutron beam during five separate visits over the past 3 years while using six unique Teledyne detector chips. We have also done 1 GeV heavy ion (Fe^{+}) measurements at the NASA Space Radiation Laboratory (NSRL), 175 MeV proton measurements at the Loma Linda University Medical Center (LLUMC), and 1.25 MeV gamma rays (^{60}Co) at the Lawrence Livermore National Laboratory (LLNL). The LANSCE neutron beam produces approximately the dose in 1 h experienced by an aircraft flying at 12 km for 30,000 h. The neutron beam lineal energy deposition spectrum ranges from 0.4 to 1024.0 keV μm^{-1} as measured by *Gersey et al*. [2003] for eight incident neutron energy spectra test cases. We found that the Teledyne detector is very sensitive to neutrons, which make up about half the particle spectrum at aviation altitudes. The detectors all showed a strong signal in the presence of a multienergy neutron beam, and all detector responses were nearly identical, indicating a consistency of the manufacturing process. For example, a typical LANSCE test run on 17 August 2014 ran for 1.0481 h with 9289 valid data points out of 9440 total (98.40%). The measured total absorbed dose rate was 4.331 rad h^{-1} using a sampling rate of 10 Hz with airplane-equivalent shielding of 5.3 g cm^{-2} Al and 3.0 g cm^{-2} High-density polyethylene (HDPE) between the beam and the detector. The conclusion of these tests is that the TID unit is sensitive to neutrons and detects them as part of the entire particle spectrum of ionizing radiation, which is consistent with an understanding that the lower energies in the 1–800 MeV range would be the most effective ionizing particles in silicon.

Real-time and archival data files are provided using version 7.00 of the ARMAS processing code with ASCII files containing the year, month, day, hour, minute, second, Julian date, latitude (degrees), longitude (degrees), altitude (m), ARMAS Level 2 absorbed dose rate Si ($\mu Gy\, h^{-1}$), NAIRAS Level 2 absorbed dose rate Si ($\mu Gy\, h^{-1}$), ARMAS Level 3 ambient dose equivalent rate ($\mu Sv\, h^{-1}$), NAIRAS Level 3 ambient dose equivalent rate ($\mu Sv\, h^{-1}$), vertical cutoff rigidity Rc (GV), quality factor (*Q*), magnetic latitude (degrees, 2015), magnetic longitude (degrees, 2015), L shell, GOES >1 Mev protons ($p\, cm^{-2}\, s^{-1}\, sr^{-1}$) (P01), GOES >0.6 Mev electrons ($e\, cm^{-2}\, s^{-1}\, sr^{-1}$) (E06), *Dst* (nT), data quality flag (0 = verified data; 1 = unreliable dose rate; 2 = Rc undetermined; 3 = *Q* undetermined), and comments. The data files are available at the public URL http://sol.

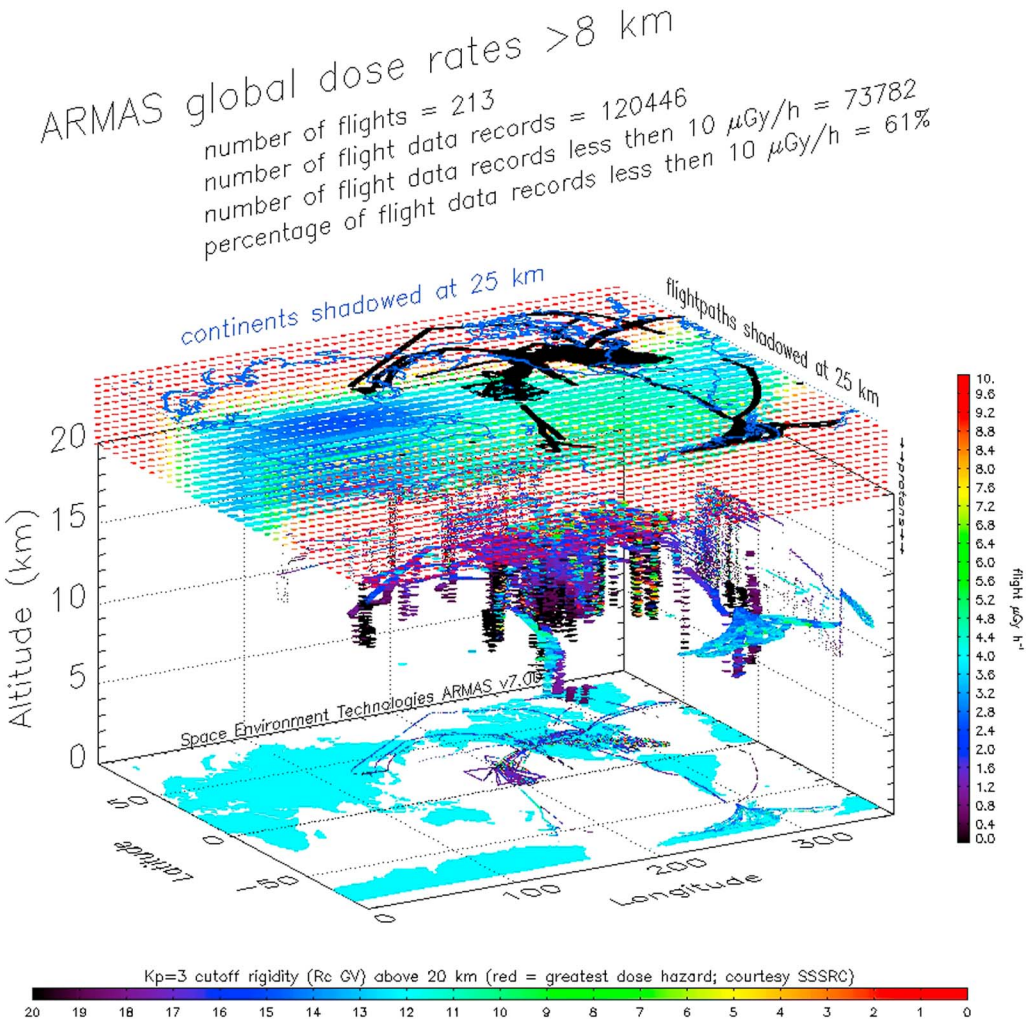

Figure 11. Global range of ARMAS measurements from all aircraft, 2013–2016, at all locations.

spacenvironment.net/~ARMAS/Level_2_3_Data.html. The metadata contains the start and end times and platform source, and NAIRAS comparison source files are identified. Each data file also contains a flag indicating whether there was NOAA Space Weather Prediction Center (SWPC) SEP event detected, the average *Kp* and *Ap*, the likelihood of a space weather event, the flight absorbed dose in Si conversion factor to dose equivalent in tissue, the flight dose equivalent in tissue normalization factor to phantom body ambient dose equivalent H*(10), the RaD-X derived conversion between TID and TEPC, the L1 flight total measured absorbed dose in Si (μGy), the L2 maximum flight measured absorbed dose rate in Si ($\mu Gy\,h^{-1}$), the L2 maximum NAIRAS modeled absorbed dose rate in Si ($\mu Gy\,h^{-1}$), the L3 flight total estimated ambient dose equivalent (μSv), the L3 maximum flight measured ambient dose equivalent rate in Ti ($\mu Sv\,h^{-1}$), the L3 maximum NAIRAS modeled ambient dose equivalent rate in Ti ($\mu Sv\,h^{-1}$), the flight mean quality factor for the range of cutoff rigidities, and uncertainties for all parameters.

The absorbed dose (L1) is calculated as L0 dose × the RaD-X derived conversion between TID and TEPC (C3). The absorbed dose rate (L2) is the time derivative of the L1 dose. The ambient dose equivalent rate (L3) is calculated as absorbed dose rate × C1 × C2 × Q_{Rc}. C1 = 1.23 and is the absorbed dose in silicon conversion factor to dose equivalent in tissue. C2 = 1.00 and is the dose equivalent in tissue normalization factor to phantom body ambient dose equivalent, H*(10). We note that for major SEP events (none discussed in this paper) the energy spectrum is unique in each case and usually much softer (different) than the background GCR spectrum. Thus, GCR-related H*(10) is not appropriate for SEP events; the results shown in this paper are primarily for cases predominantly experiencing the GCR background, although other energy deposition processes

Table 2. ARMAS FM Flight Dosimetry Result Summary (V7.00)[a]

	NASA AFRC DC-8 FM1 Case 1	NSF NCAR G-V FM2 Case 2	NOAA AOC G-IV FM2 Case 3	Commercial FM5 Case 4	NASA AFRC ER-2 FM3 Case 5
Region	High-latitude North America	High-latitude South America & Antarctica	Low-latitude Hawaii & Pacific	Midlatitude CONUS	Midlatitude Western U.S.
Start UT	2013/08/27 at 18:01	2015/10/03 at 11:30	2016/02/03 at 19:58	2016/02/10 at 21:42	2015/09/09 at 16:09
End UT	2013/08/28 at 02:53	2015/10/04 at 00:34	2016/02/04 at 03:48	2016/02/11 at 03:24	2015/09/09 at 16:55
Duration (h)	11.8	13.1	7.8	5.7	0.8
Maximum absorbed dose rate (μGy h^{-1})	4.70	7.40	1.78	2.94	4.12
Total absorbed dose (μGy)	10.19	37.24	6.27	5.10	7.84
Maximum ambient dose equivalent rate (μSv h^{-1})	11.97	18.86	3.36	7.34	9.76
Total ambient dose equivalent (μSv)	25.94	94.86	11.87	12.71	18.59
Mean *Q*	2.07	2.07	1.54	2.03	1.93
Maximum altitude (m)	12900	12300	14400	10973	17300
|Maximum & minimum| latitude (deg)	50.20 29.40	−53.10 −75.28	21.30 4.00	39.90 33.95	35.20 34.60
|Maximum & minimum| longitude (°E)	−117.60 −95.10	−70.90 −60.20	−158.00 −144.10	−118.33 −77.50	−118.20 −113.40
|Maximum & minimum| magnetic latitude (deg)	58.47 38.17	−65.74 −43.50	21.75 5.91	49.25 40.33	41.73 41.00
|Maximum & minimum| magnetic longitude (°E)	−53.94 −25.11	8.19 1.32	−89.26 −72.77	−51.19 −5.75	−51.27 −46.00
Maximum, minimum Rc (GV)	4.28, 0.48	3.89, 0.24	12.64, 11.20	4.43, 1.74	4.12, 3.80
Maximum, minimum *L*	3.66, 1.62	5.92, 1.90	1.16, 1.01	2.35, 1.72	1.80, 1.76
Maximum & minimum GOES >1 MeV proton flux (# cm^{-2} s^{-1} sr^{-1})	3.24E+00 2.85E+00	1.25E+02 2.19E+00	1.75E+00 4.59E−01	4.50E+00 6.10E−01	1.12E+01 4.74E+00
Maximum & minimum GOES >0.6 MeV electron flux (# cm^{-2} s^{-1} sr^{-1})	5.40E+03 5.36E+03	2.50E+04 1.32E+02	2.34E+03 1.11E+03	4.41E+04 2.38E+04	2.55E+04 1.12E+04
|Maximum, minimum| *Dst* (nT)	−54, −37	−24, −11	−16, −6	−19, −13	−88, −79
mean *Kp*, mean *Ap*, NOAA G	2 9 G2	3 22 G1	2 6 G1	2 11 G1	3 12 G3
Space weather	low	moderate	low	low	low

[a]Dates are formatted as year/month/day.

(charged particle precipitation and gamma ray flashes) may play a role. The RaD-X TEPC and TID average absorbed dose rate ratio is C3 = 1.40 from *Mertens et al*. [2016]; this was also reported by *Hands and Dyer* [2009] and is consistent with the theoretically determined 1.33 ratio [*Schwadron et al*., 2012]. Rc is calculated as a function of epoch-dependent *Kp*, latitude, longitude, and altitude.

We determine the quality factor, *Q*, as a function of Rc using a second-degree polynomial fit for the results of *Burda et al*. [2013] in the relationship of equation (1) (Figure 10). These were verified with independent TEPC measurements of *Q* versus Rc in the ARMAS Phase I work during 2011 (Table 1).

$$Q_{Rc} = 2.175 - 0.066\ Rc + 0.001\ Rc^2 \quad (1)$$

The RMS 1 sigma uncertainty budget for ARMAS L3 data is as follows: (i) *Mazur et al*. [2011] micro dosimeter detector systematic measurement uncertainty ($a_1 = \pm 20\%$) in L0 and L1 data; (ii) dose rate calculation uncertainty ($a_2 = \pm 5\%$) in L2 data; (iii) absorbed dose in silicon conversion factor to dose equivalent in tissue uncertainty ($a_3 = \pm 2.3\%$) in L3 data; (iv) conversion to normalized ambient dose equivalent uncertainty, i.e., H*(10) operational quantity for area monitoring ($a_4 = \pm 0\%$ under predominantly GCR source radiation) in L3 data;

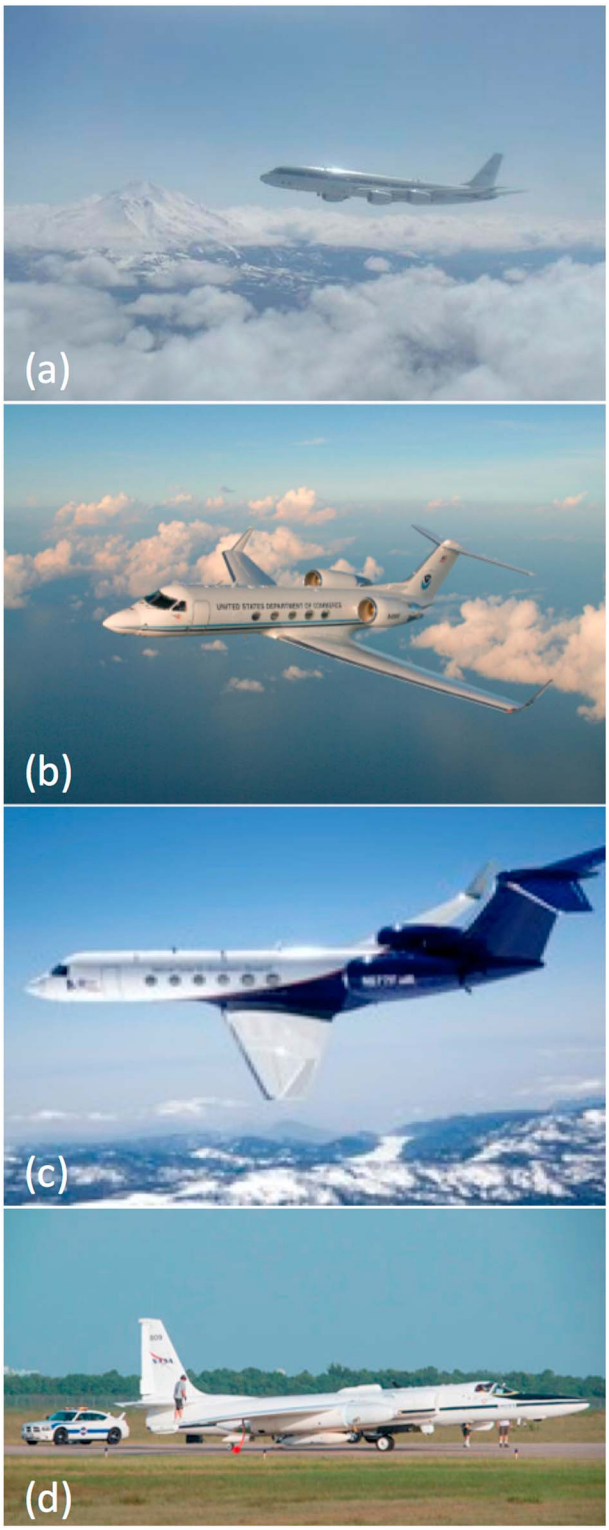

Figure 12. (a) NASA AFRC DC-8, (b) NOAA Gulfstream IV-SP, (c) NSF/NCAR Gulfstream V, and (d) NASA AFRC ER-2.

(v) Rc modeled with *Kp* using a polynomial fit uncertainty ($a_5 = \pm 10\%$) in L3 data; (vi) *Burda et al.* [2013] polar to equatorial change in *Q* using a polynomial fit uncertainty ($a_6 = \pm 3.6\%$) in L3 data; (vii) Q_{Rc} modeled with Rc using a polynomial fit uncertainty ($a_7 = \pm 5\%$) in L3 data; and (viii) *Mertens et al.* [2016] RaD-X conversion between TID and TEPC uncertainty ($a_8 = \pm 2\%$) in L3 data. The total ARMAS Level 2 absorbed

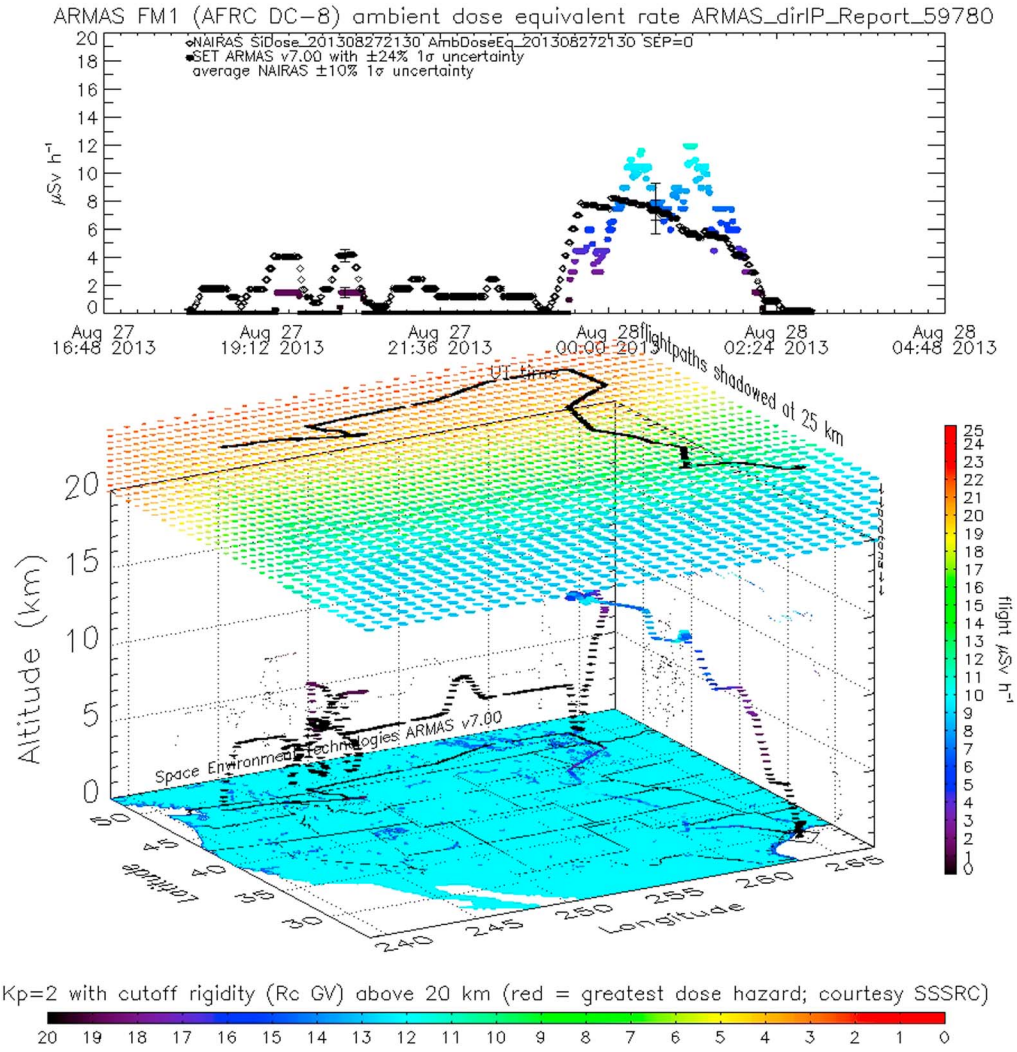

Figure 13. The 27–28 August 2013 ARMAS FM1 DC-8 measurements along near-constant longitude.

dose rate in silicon RMS measurement uncertainty is $\sigma_{L2} = \sqrt{(a_1{}^2 + a_2{}^2 + a_8{}^2)} = \pm 20.7\%$. The total ARMAS Level 3 ambient dose equivalent rate calculation RMS measurement plus derived quantity uncertainty is $\sigma_{L3} = \sqrt{(a_1{}^2 + a_2{}^2 + a_3{}^2 + a_4{}^2 + a_5{}^2 + a_6{}^2 + a_7{}^2 + a_8{}^2)} = \pm 23.9\%$.

4. Measurement Results

Figure 11 shows the global range of ARMAS measured absorbed dose rate in silicon Level 2 data from six FM instruments by latitude, longitude, and altitude >8 km. Our 213 flights occurred between May 2013 and October 2016. Below 8 km, the FM instrument is generally insensitive to the much reduced radiation environment. In Figure 11, the color-coded Rc values calculated with $Kp = 3$ are shown above 20 km. There are 120,446 individual data records with about 61% of the records having absorbed dose rate values $<10\ \mu Gy\ h^{-1}$. Higher dose rates are likely due to operational factors since most of these instruments are flying piggyback on research aircraft that are laden with racks of other flight instruments. It is possible that radio frequency interference (RFI) from other instruments or environmental phenomena, e.g., lightning in hurricanes, has caused significant interference on some flights, and we presently exclude those data from scientific analysis.

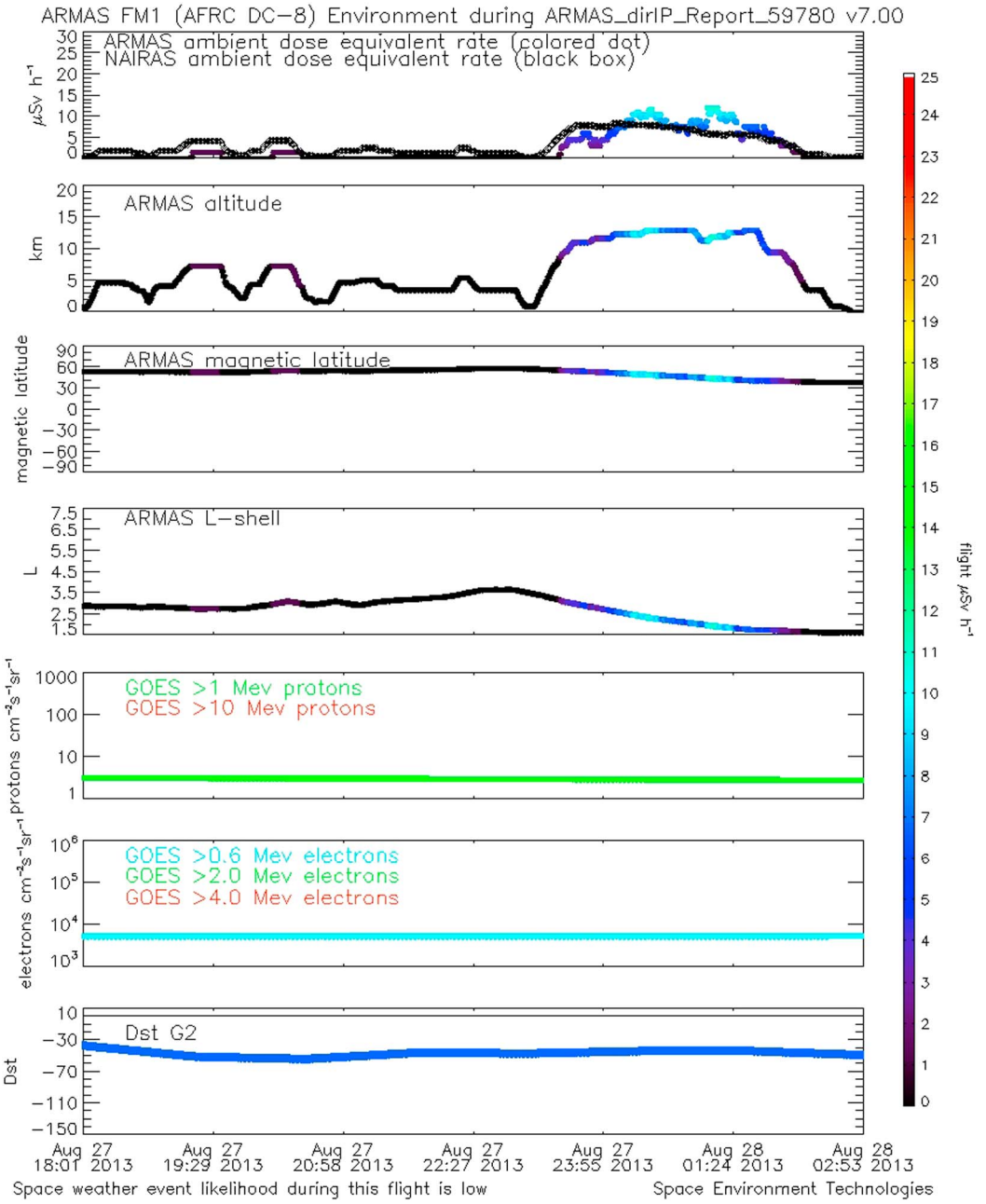

Figure 14. Environmental conditions during 27–28 August 2013 ARMAS FM1 DC-8 flight.

We show cases from five representative flights that are summarized in Table 2. Figure 12 shows the research aircraft used by ARMAS but not including commercial carry-on flights on B-737, B-747, B-757, B-777, A-319, A-320, and Q200 aircraft. These are, in order from top to bottom, the NASA AFRC DC-8, NOAA G-IV, NSF/NCAR G-V, and NASA AFRC ER-2.

4.1. Case 1: Nearly Constant Longitude and Range of Magnetic Latitudes During Minor Radiation Event

This flight (Figure 13) is an example of the type of piggyback opportunities our team used to obtain dose rate measurements. The primary science mission of this DC-8 flight was to sample the 2013 Yosemite Rim fire smoke plume from California through Idaho into Canada. On 27 August 2013 the DC-8 aircraft departed Spokane and flew northeast/east at low altitudes (3–7 km) between Spokane and Winnipeg to sample as

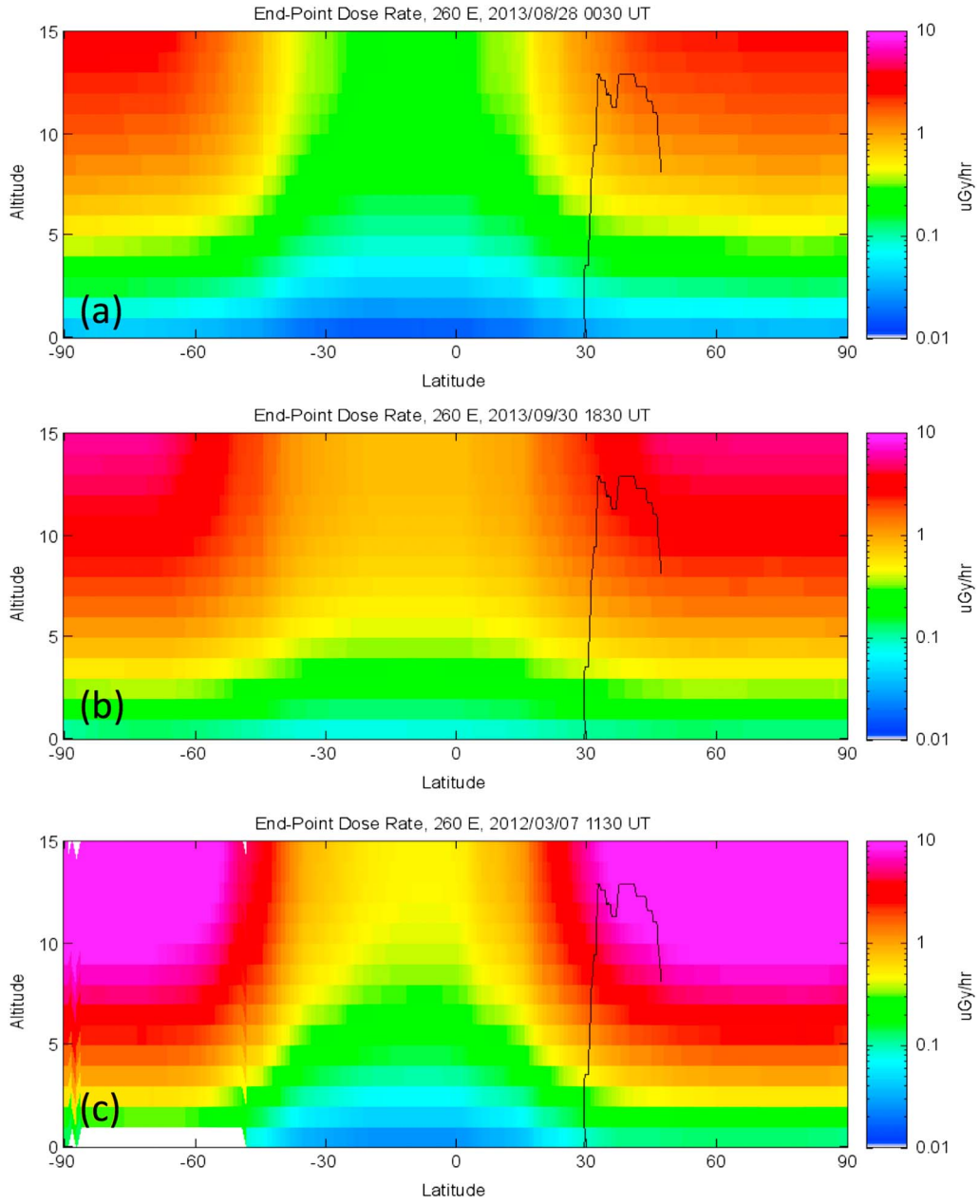

Figure 15. (a) The 27–28 August 2013 DC-8 flight from Winnipeg to Houston during minor radiation event with NAIRAS longitude slice; (b) NAIRAS S2 event; and (c) NAIRAS S3 event.

much smoke as possible and then flew high altitudes (11–12 km) to transit from Winnipeg to Houston. This latter segment was designed to study tropical and extratropical air masses in a high-altitude anticyclone region over the central U.S.

The data duration was 11.8 h between 27 August at 18:01 UT and 28 August at 02:53 UT. The maximum absorbed dose rate was 4.7 μGy h^{-1}. The average *Kp* was 2 (*Ap* = 9), the flight total measured absorbed dose in Si was 10.2 μGy, the total ambient dose equivalent was 25.9 μSv, and the mean quality factor for the range of cutoff rigidities (4.28–0.48) was 2.07. A minor radiation enhancement period occurred during this flight (28 August 2013 at 00:10–01:40 UT) from an unknown source with *Dst* −44 nT, low > 1 MeV GOES proxy proton fluxes, and *L* = 2.5–1.7 (Figure 14). Figure 15 shows a slice of the NAIRAS data for this flight (Figure 15a) in comparison with an S2 event captured by NAIRAS on 30 September 2013 (Figure 15b) and an S3 event by

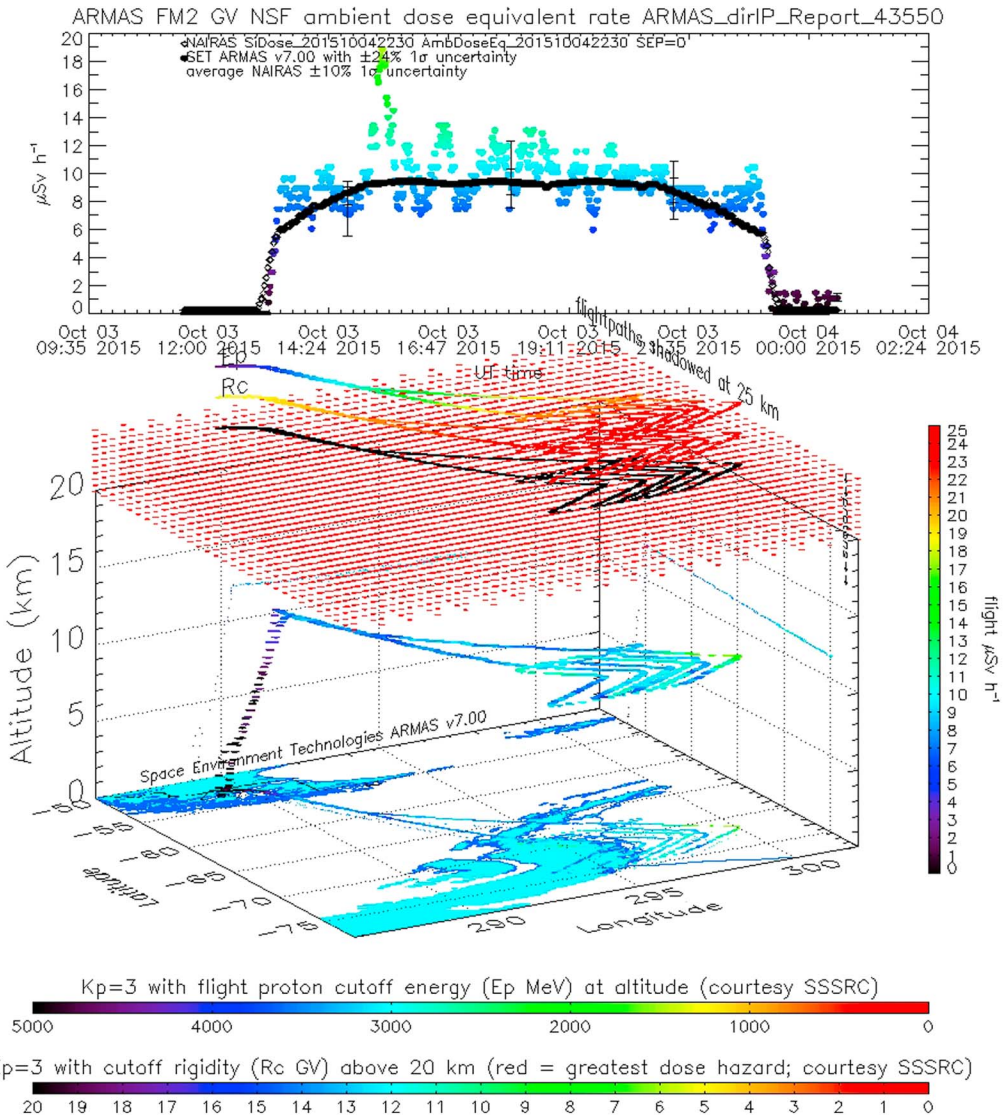

Figure 16. The 3–4 October 2015 ARMAS FM2 NSF/NCAR G-V measurements at high magnetic latitudes.

NAIRAS on 7 March 2012 (Figure 15c). These measurements provide an estimate of the ambient dose equivalent rate increasing from 4 to 12 μSv h^{-1}, comparable to NAIRAS results, for minor radiation events between 50° and 40° magnetic latitudes and also suggest the potential for higher dose rates during larger radiation storms.

4.2. Case 2: High (Southern West Hemisphere) Magnetic Latitudes

The NSF/NCAR G-V science mission (Figure 16) studied the Antarctic ice shelf thickness. On 3 October 2015 the G-V departed southern Chile and flew south at high altitudes (11–12 km) to arrive above the ice shelf.

The data duration was 13.1 h between 3 October at 11:30 UT and 4 October at 00:34 UT. The maximum absorbed dose rate was 7.4 μGy h^{-1}. The average *Kp* was 3 (*Ap* = 22), the flight total measured absorbed dose in Si was 37.2 μGy, the total ambient dose equivalent was 94.9 μSv, and the mean quality factor for the range of cutoff rigidities (3.89–0.24) was 2.07. Shown as proxy data, a small proton event peaked on 3 October 2015 at 15:23 UT with >1 Mev proxy protons reaching 125 particles cm^{-2} s^{-1} sr^{-1} when the aircraft was at −61.6° magnetic latitude (*L* = 4.4) and *Dst* = −24 nT (Figure 17). The flux of higher-energy protons at GOES was not significant, and we do not indicate that these particular protons were the cause of the higher dose rates.

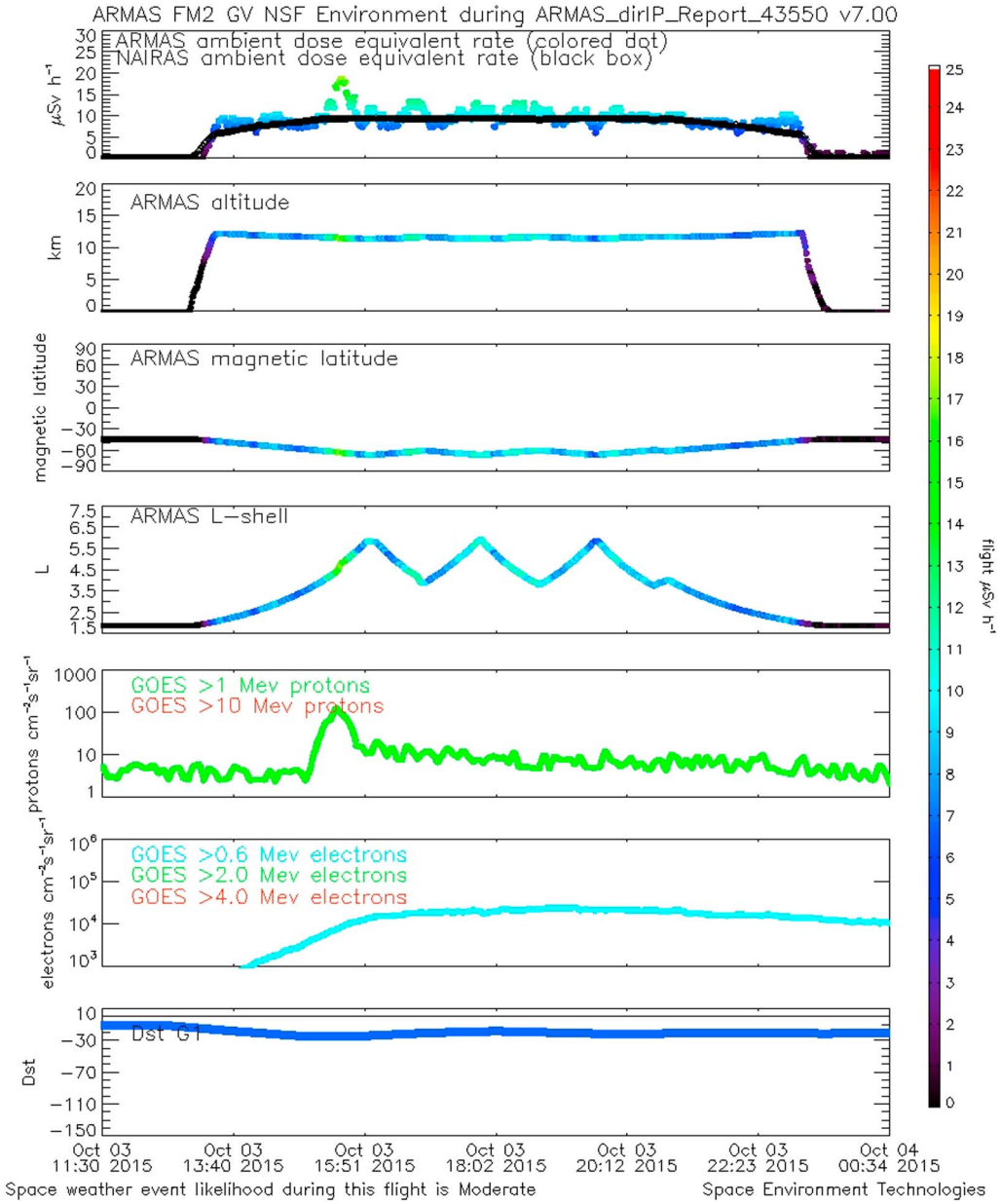

Figure 17. Environmental conditions during 3–4 October 2015 ARMAS FM2 NSF/NCAR G-V flight.

The peak dose rate occurred at 15:28 UT, $L = 4.8$, and −62.8° magnetic latitude, reaching background at 15:45 UT (−64.6°). This mesoscale region of enhanced radiation took approximately a half hour to fly through at constant altitude, and we suggest that an analogy might be flying through a radiation cloud. This is not an entirely new phenomenon. For example, *Lee et al.* [2015] measured temporal radiation variations on aircraft under constant flight conditions. It is highly unlikely that the dose rate enhancements are SEP-related and the minor *Dst* disturbance suggests a possible geomagnetic modulation of the GCRs as one pathway for creating these dose rate peaks. Another intriguing suggestion is that this radiation enhancement could be from energetic electrons or O^+ precipitating into higher altitudes from the outer radiation belt due to electromagnetic ion cyclotron (EMIC) waves (A. Halford, private communication, 2016). In addition, backscattered albedo electrons (J. Adams, private communication, 2016) may contribute radiation at higher altitudes than this flight as well as gamma rays from large storm or hurricane lightning, and sprite events may contribute to a radiation field enhancement. The Case 2 higher dose rates did not occur at altitudes where albedo electrons are

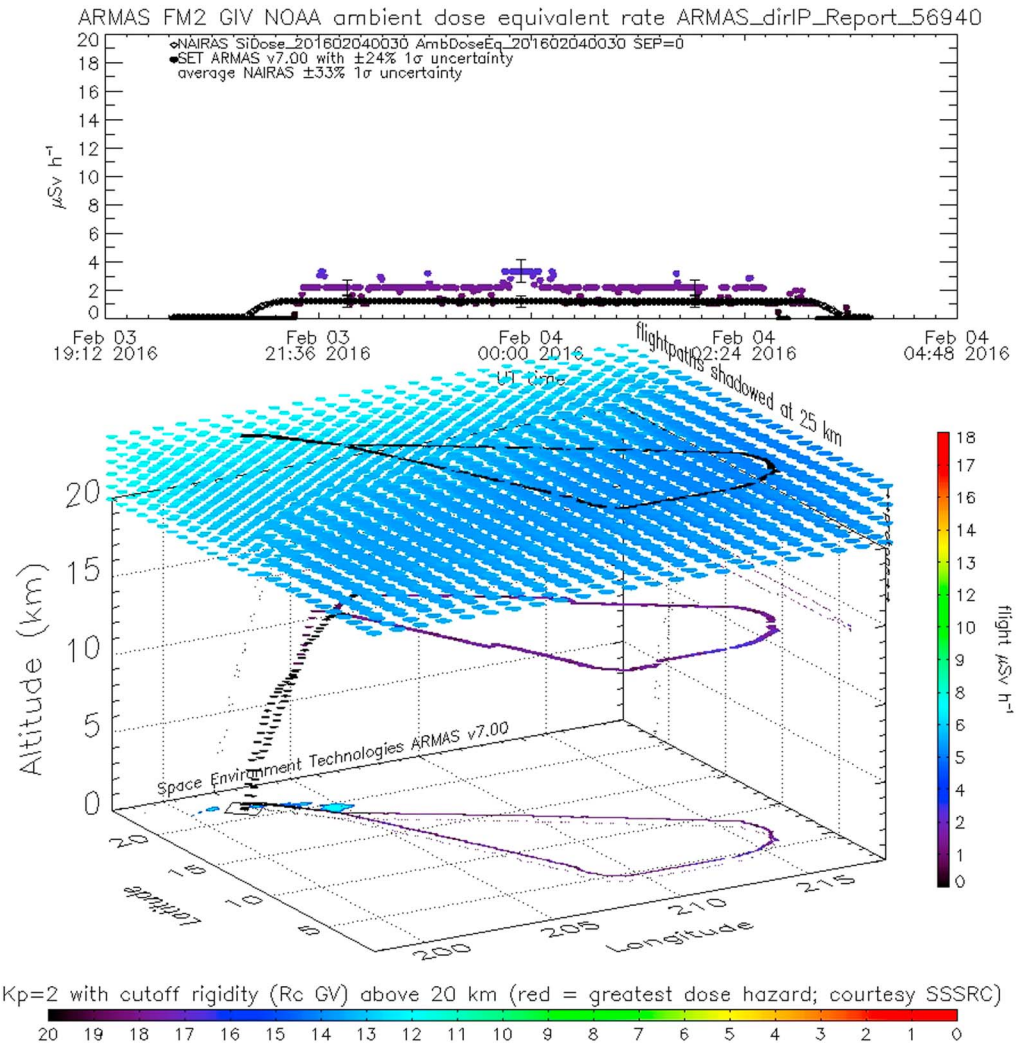

Figure 18. The 3–4 February 2016 ARMAS FM2 NOAA G-IV measurements at low magnetic latitudes.

expected, nor was the flight in the vicinity of a large tropospheric storm. This case deserves detailed study beyond the scope of this paper. Ambient dose equivalent rates increased from 8.7 to 18.9 μSv h^{-1} at commercial altitudes (11.5 km) for this event, demonstrating an ARMAS sensitivity to variability in low-level space weather-driven phenomena and suggesting at least 8 μSv h^{-1} dose rates for southern high-latitude commercial flights. The Level 3 ARMAS FM2 uncertainty is 23.9%, and the peak of the cloud event radiation at 18.86 μSv h^{-1} was almost 5σ ($8.68 \times (1 + 5 \times 0.239) = 19.05$ μSv h^{-1}) above the prior background measurements.

4.3. Case 3: Low (Equatorial Pacific) Magnetic Latitudes

The NOAA G-IV primary science mission (Figure 18) was to study the equatorial Pacific ocean-atmosphere coupling during the 2016 El Niño event. On 3 February 2016 the G-V aircraft departed Hawaii and flew south at high altitudes (>13 km) to arrive above the equatorial Pacific.

The data duration was 7.8 h between 3 February at 19:58 UT and 4 February at 03:48 UT. The maximum absorbed dose rate was 1.8 μGy h^{-1}. The average *Kp* was 2 (*Ap* = 6), the flight total measured absorbed dose in Si was 6.3 μGy, the total ambient dose equivalent was 11.9 μSv, and the mean quality factor for the range of cutoff rigidities (12.64–11.20) was 1.54. There was no space weather event during the flight; the aircraft was between 21° and 6° magnetic latitudes and $L = 1.1$–1.0 with *Dst* from −16 to −6 nT (Figure 19). This flight suggests a lower boundary condition for the minimum ambient dose equivalent rates of 2 μSv h^{-1} at business jet altitudes of 13.8–14.4 km in equatorial regions and half that at lower commercial altitudes (measured as the aircraft passed through 11 km) when there is no significant space weather activity.

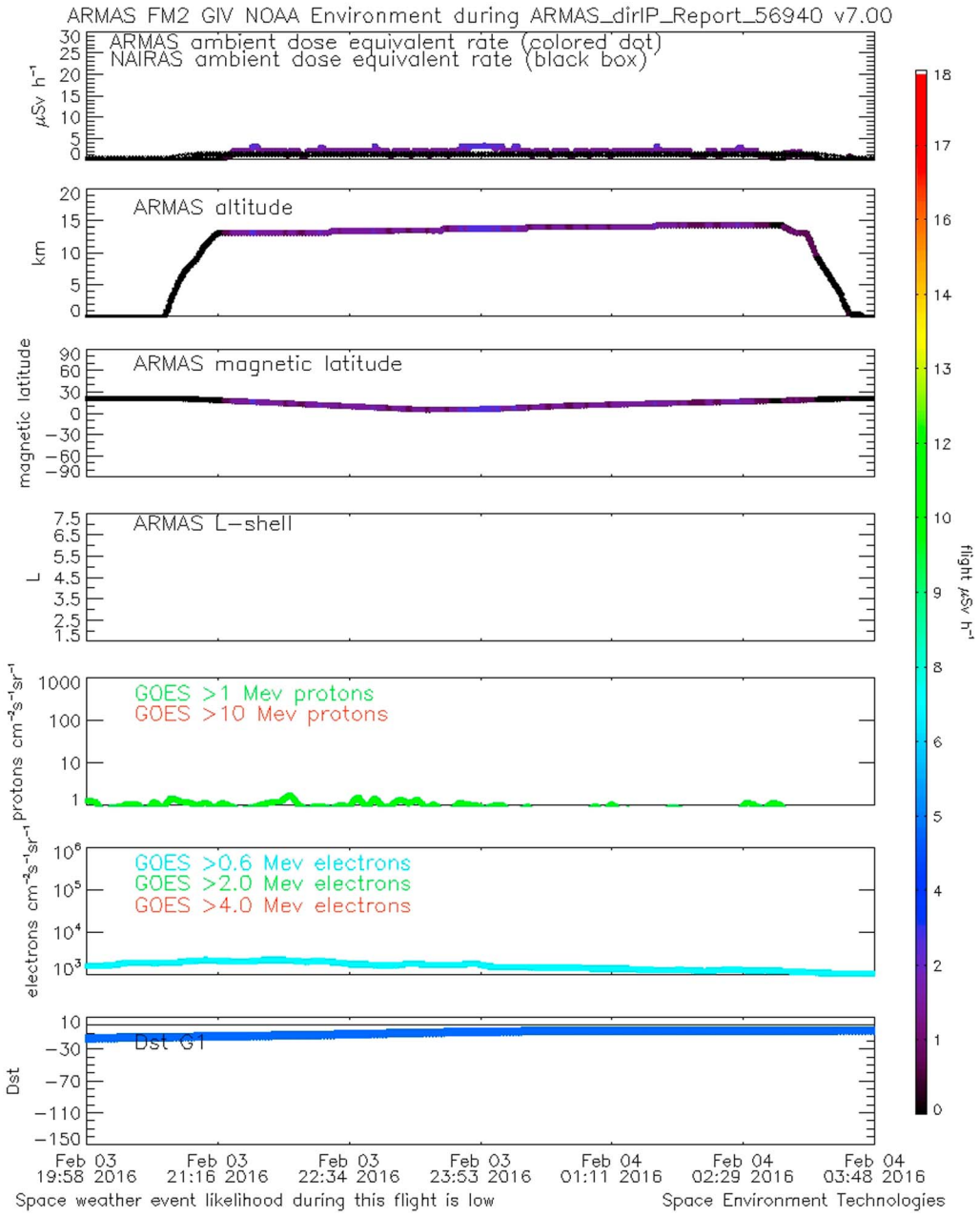

Figure 19. Environmental conditions during 3–4 February 2016 ARMAS FM2 NOAA G-IV flight.

4.4. Case 4: Typical CONUS

This ARMAS flight (Figure 20) used a carry-on, self-contained FM5 unit on a commercial carrier between Washington, District of Columbia, and Los Angeles, California. On 10–11 February 2016 the aircraft departed Dulles International Airport and flew southwest at high altitude (10.9 km) across the United States.

The data duration was 5.7 h between 10 February at 21:42 UT and 11 February at 03:24 UT. The maximum absorbed dose rate was 2.9 μGy h^{-1}. The average *Kp* was 2 (*Ap* = 11), the flight total measured absorbed dose in Si was 5.1 μGy, the total ambient dose equivalent was 12.7 μSv, and the mean quality factor for the range of cutoff rigidities (4.43–1.74) was 2.03. There was no space weather event during the flight while the aircraft was between 49° and 40° magnetic latitudes and *L* = 2.3 to 1.7 with *Dst* −13 to −19 nT (Figure 21). This flight suggests a lower boundary condition for the minimum ambient dose equivalent rates of 4 μSv h^{-1} at

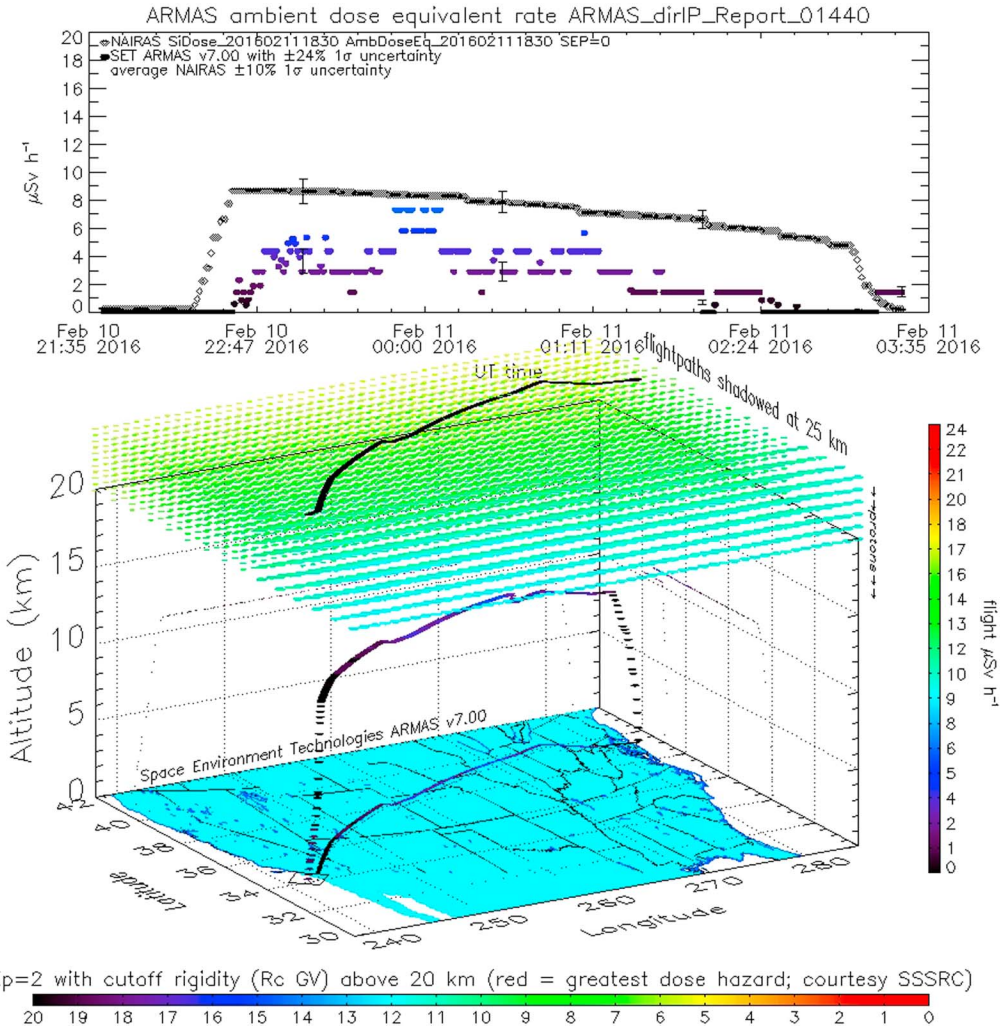

Figure 20. The 10–11 February 2016 ARMAS FM5 commercial flight measurements across CONUS.

commercial altitudes of 11 km in midlatitude CONUS regions when there is no significant space weather activity. This is half the peak dose rate in Case 1 when there was a small radiation event.

4.5. Case 5: RaD-X Campaign Support

The primary science mission of the NASA AFRC ER-2 flight on 9 September 2015 (Figures 22 and 23) was to support the NASA RaD-X high-altitude balloon flight on 25 September 2015 [*Mertens et al*., 2016; *Straume et al*., 2016; *Meier et al*., 2016]. The ER-2 carried two instruments, i.e., the TEPC described by *Mertens et al*. [2016] in the wing pod and the ARMAS FM3 in the Q-bay. The ARMAS FM3 instrument was not flown on the RaD-X balloon but shares the common selection of the Teledyne μDos chip as the detector. Both the RaD-X and FM3 μDos chips were compared in laboratory beam lines at LANSCE, LLUMC, and LLNL and were found to have nearly identical responses. The electronics packages for the RaD-X and FM3 instruments are different, the former built by NASA LaRC and the latter by SET. Data comparisons are ongoing with the balloon flight data, and a useful comparison for this Case 5 flight (Figure 23 in this paper) is the 16–17 UT flight segment of *Mertens et al*. [2016] (Figure 15). In future work we will compare our measurements with the German DLR measurements on a Lufthansa flight at a Rc also near 4.1 GV [*Meier et al*., 2016]. The aircraft for the Case 5 flight departed Palmdale and flew eastward starting at 16:09 UT.

Though the flight lasted longer, the ARMAS FM3 data duration was 0.8 h on 9 September between 16:09 UT and 16:55 UT and terminated due to a microprocessor crash. The nominal operating temperature of FM3 is

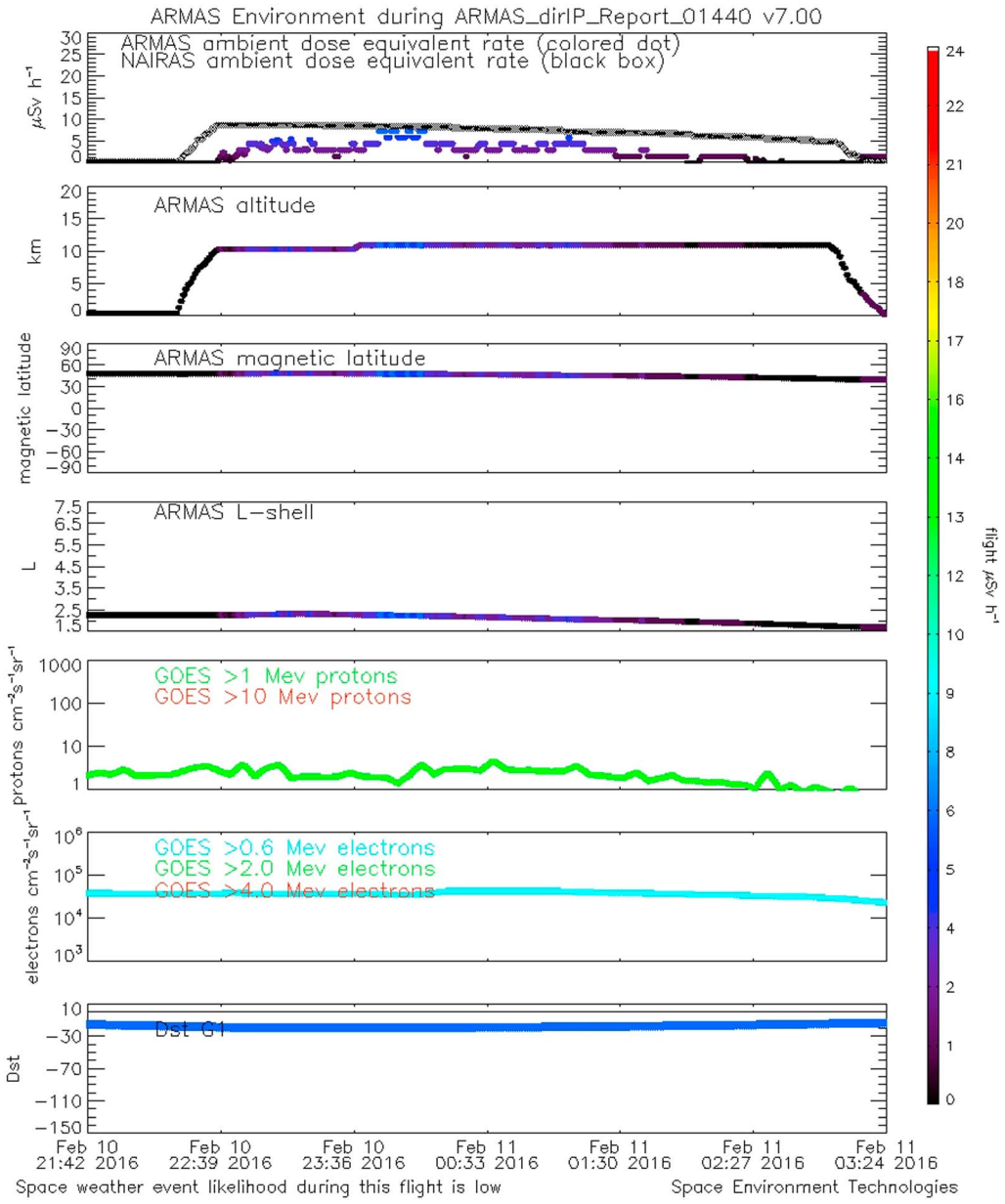

Figure 21. Environmental conditions during 10–11 February 2016 ARMAS FM5 commercial flight.

0–25°C, and the instrument was operating on the edge of its performance envelope in the ER-2 Q-bay where the temperature at altitude can easily be −30°C. The maximum absorbed dose rate was 4.1 μGy h^{-1}. The average *Kp* was 3 (*Ap* = 12), the flight total measured absorbed dose in Si was 7.8 μGy, the total ambient dose equivalent was 18.6 μSv, and the mean quality factor for the range of cutoff rigidities (4.12–3.80) was 1.93. There was a G2–G3 moderate space weather event during the flight while the aircraft was at 17.3 km and 41.5° magnetic latitude (*L* = 1.8) with *Dst* −88 to −79 nT (Figure 24). This flight occurred over similar magnetic latitudes to RaD-X but at a lower altitude below the Pfotzer maximum. Compared to the TEPC on the ER-2 that had an adjusted absorbed dose rate of 4.2 μGy h^{-1} during the start of the flight when FM3 was active, the FM3 measured 4.1 μGy h^{-1}. This includes the TEPC-to-TID laboratory adjustment value of 1.40 from RaD-X [*Mertens et al.*, 2016] and was nearly identical to the RaD-X TEPC 17 UT measurements. FM3 showed elevated dose rates compared to NAIRAS absorbed dose rates (Figure 23) likely due to an ongoing minor geomagnetic storm during the flight. This suggests that additional charged particles may have found their way onto

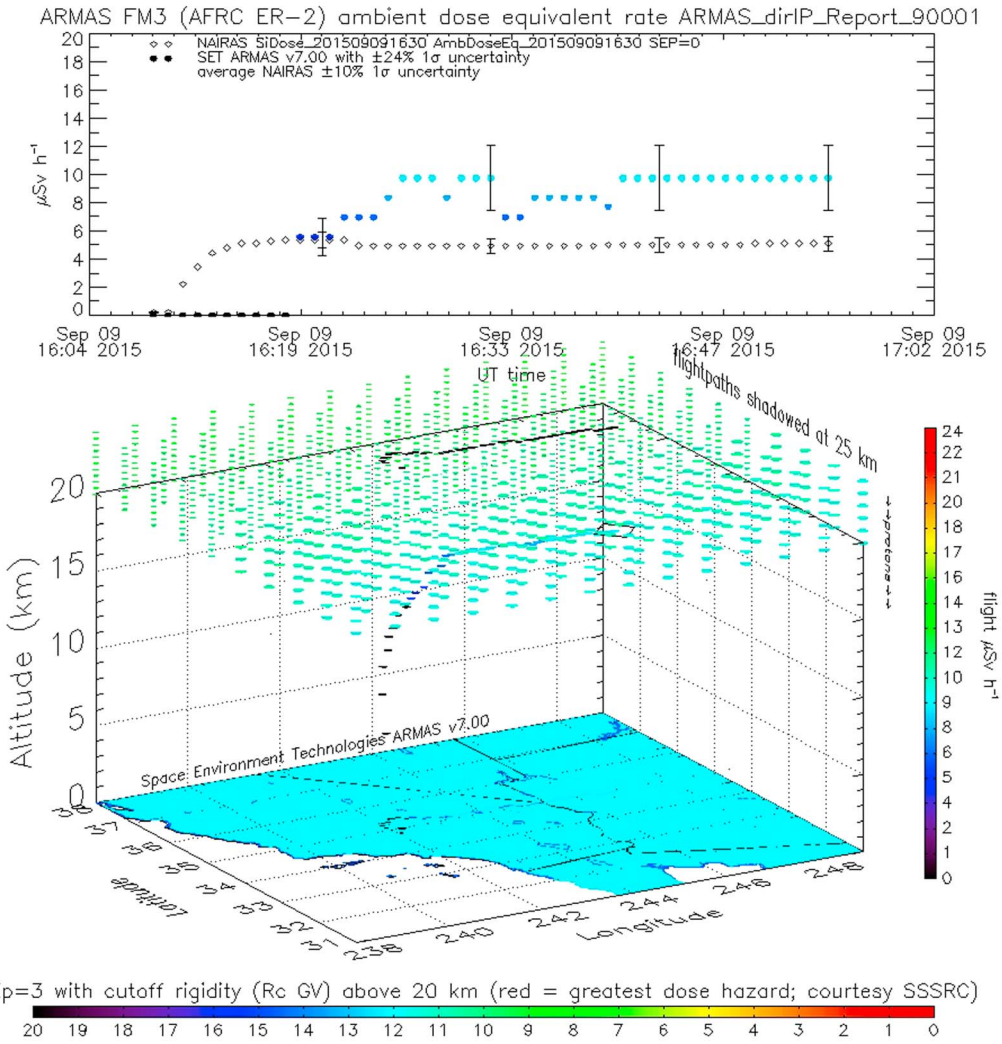

Figure 22. The 9 September 2015 NASA AFRC ARMAS FM3 ER-2 Level 3 measurements supporting RaD-X.

midlatitude magnetic field lines during geomagnetic storm conditions and could elevate the dose rate compared to background levels.

5. Discussion

The ARMAS team has successfully achieved an initial goal of building a small fleet of instruments to measure the ambient radiation environment at commercial aircraft altitudes at any point on the planet, transmit the data to the ground in real time, and provide quality ambient dose equivalent rates such as the Level 3 data product that is comparable to NAIRAS. Latency to users is 5 min to 15 min, depending upon the FM instrument used. Two hundred thirteen flights, on 11 different research and commercial aircraft, have provided 120,446 unique time records. The ARMAS data records over 3 years are comparable in scope to the decade-long Liulin data set [*Ploc et al.*, 2013], which is available online at http://hroch.ujf.cas.cz/~aircraft/ and contains 3699 flights with 133,438 H*(10) records with 5 min resolution covering one solar cycle from 2001 to 2011.

Since NAIRAS performs hourly prototype operational modeling of the data-driven climatology of the global radiation environment at current epoch, our task has been both to provide a validation of NAIRAS through data measurements, partially achieved with these ARMAS measurements, and to demonstrate the possibility of a future TID data stream for assimilation. This will help the commercial aviation community achieve radiation weather safety, as opposed to relying on radiation climatology as is currently done.

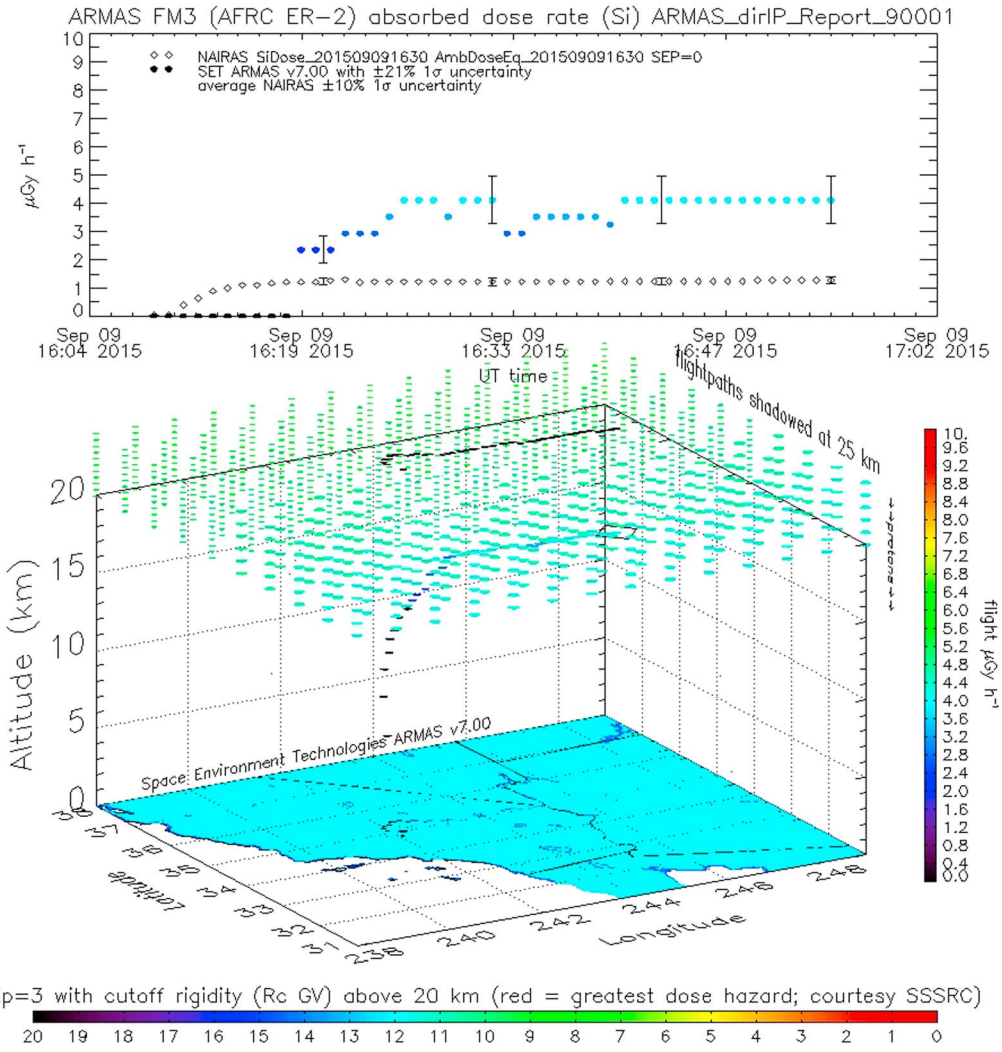

Figure 23. The 9 September 2015 NASA AFRC ARMAS FM3 ER-2 Level 2 measurements supporting RaD-X.

5.1. Radio Frequency Interference and Other Data Artifacts

ARMAS instruments fly piggyback on research aircraft and as carry-on units on commercial flights. The Teledyne detector is sensitive to external, man-made electromagnetic radiation, generically called "RFI" here. For example, placing a smartphone "Flashlight" strobe within a few centimeters of the micro dosimeter can produce a repeatable, high dose rate. There is a location at Los Angeles International Airport (LAX) where the primary author can sit at a terminal café prior to boarding a flight and repeatedly measure unusually high dose rates while less than 100 m above sea level. Additionally, on some research aircraft during take-off the ARMAS instrument can see abnormally high dose rates. The duration of these man-made RFI flight events is typically only a few minutes, and the source of the interference is unidentified. It is possible that the Teledyne chip experiences a "microphone effect" where noise in the output is generated from vibration of the silicon plate of the detector due to acoustic frequencies. This would be consistent with a loud acoustic environment near take-off and landing, i.e., times when we often see this interference. Research aircraft usually carry many instruments, sometimes changing from flight to flight, and these may create unintended interference. Finally, there is a location in the middle of the Gulf of Mexico where we have continuously seen abnormally high dose rates during several research flights most probably from external RFI.

There may be environmental factors that affect ARMAS measurements in some cases. We note that during the 2015 hurricane observing season when ARMAS was flying piggyback on research aircraft, there were

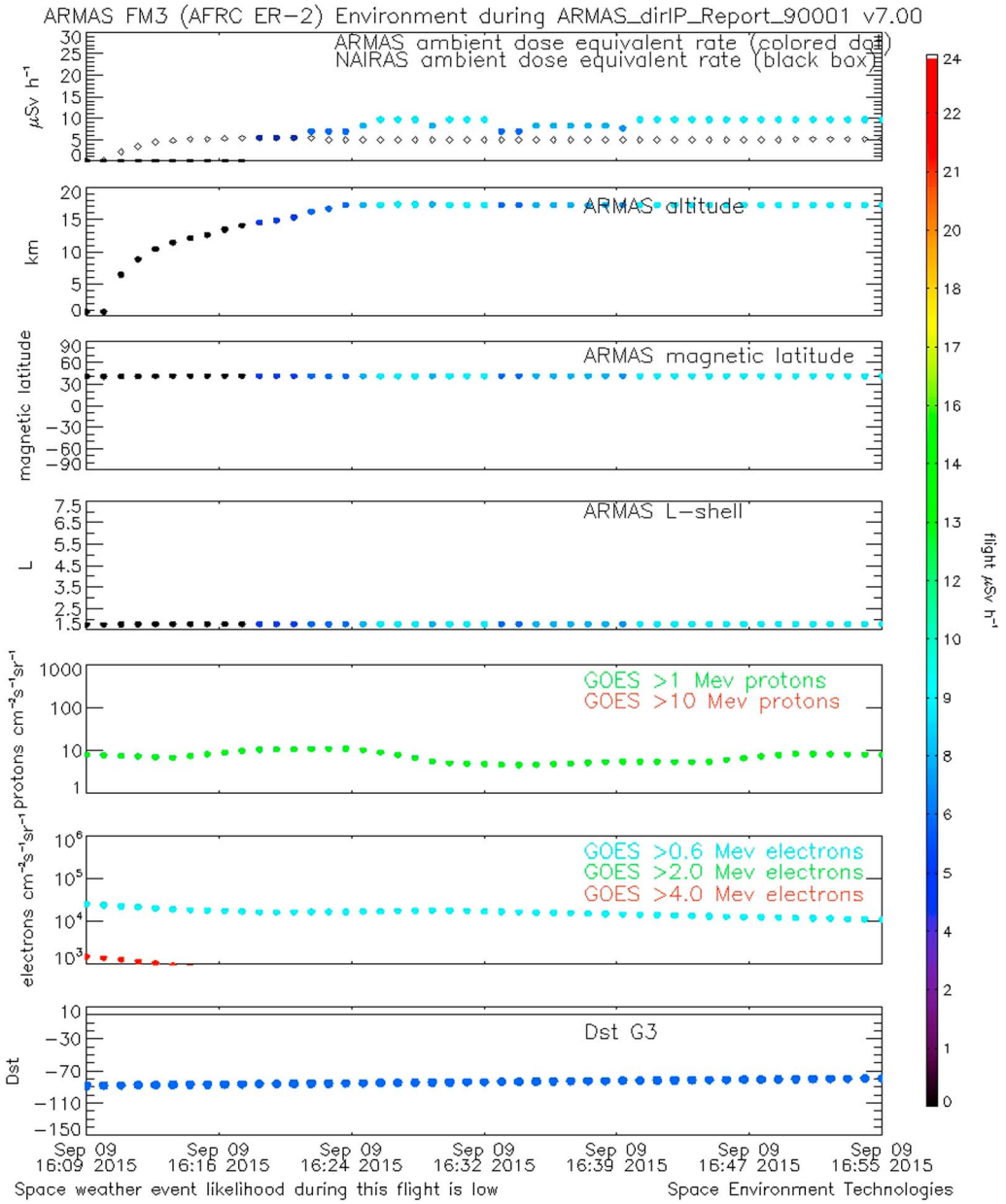

Figure 24. Environmental conditions during 9 September 2015 NASA AFRC ARMAS FM3 ER-2 flight.

unknown high dose rates while the aircraft was flying over, above, through, and near the hurricanes themselves. It is possible, but not verified, that terrestrial gamma ray flashes (TGFs) were measured by ARMAS.

We have thoroughly grounded our instrument electronics when attached to the aircraft and have taken additional steps to ensure a constant DC voltage input to the detector that is well above the threshold of 13 VDC. All measurements, except those on the ER-2, were conducted while the instrument was at cabin temperature (15–25°C) and pressure (1800–2400 m). On the ER-2, the Q-bay is at 9144 m (30,000 ft.) equivalent pressure, and the temperature is near −30°C. We believe that the shortened measurement time in Case 5 compared to the flight length was consistent with a microprocessor (not μDos micro dosimeter) crash related to operations in a temperature regime outside the nominal performance envelope for the COTS microprocessor chip.

Highly suspect data due to RFI or other sources is labeled during the Level 3 data processing. Unusually high dose rates are defined as those above 10 μGy h^{-1} when no SEP events are occurring. These data are of engineering and possible science interest to the team, but we typically remove these data from scientific analysis.

As noted above, we have been able to conduct some flights in conjunction with the TEPC instrument and data comparisons will continue. We expect further results to be a topic of a separate paper. We also recognize that NAIRAS is only one model against which we can compare ARMAS. The International Commission on Radiation Units and Measurements (ICRU) standard data set [*ICRU*, 2011] along with Predictive Code for Aircrew Radiation Exposure (PCAIRE), Korean Radiation Exposure Assessment Model (KREAM), or other models could potentially provide further insights, and we look forward to collaborations with those communities in future studies.

5.2. Space Weather Radiation Events

ARMAS has measured variability of dose rates at aviation altitudes that can be attributed to space weather activity. Space weather is the shorter-term variable impact of the Sun's photons, solar wind particles, and interplanetary magnetic field upon the Earth's environment that can adversely affect technological systems. It is not the climatological solar cycle modulation of GCRs. In addition to large-scale (hemispheric) radiation variation during SEP events and global scale GCR radiation that affects the entire planet, we have now observed radiation variability in small mesoscale regions. For example, Case 2 shows that a small radiation cloud may exist that can double the dose rate within a unique high magnetic latitude and longitude mesoscale region. The source of these mesoscale radiation enhancements is possibly from non-SEP and GCR particles and photons, including higher-altitude, higher-latitude precipitation from outer belt relativistic electrons that then may create lower altitude secondary and tertiary radiation regions. Ambient dose equivalent rates increased from 8.7 to 18.9 $\mu Sv\,h^{-1}$ at commercial altitudes (11.5 km) for Case 2, demonstrating sensitivity of the ARMAS system to variability in space weather, i.e., higher particle or photon fluxes that, in this case, may be associated with EMIC waves. The radiation region extended across 4° of magnetic latitude and lasted for 31 min of flight time. Case 5 suggests that active geomagnetic conditions may also modify the magnetospheric magnetic field and/or change the L shell/cutoff rigidity to sufficiently increase a particle-induced radiation environment at high altitudes and midlatitudes.

5.3. GCR Background

In the context of the GCR background radiation environment on short time scales (we are not investigating longer-term solar cycle effects on dose rates in this paper), Cases 1, 2, 3, and 4 all demonstrate boundary conditions for tissue exposure at various latitude regions. For example, *when there is no significant space weather occurring*, Case 2 suggests at least a 8 $\mu Sv\,h^{-1}$ dose rate for (southern) high-latitude commercial altitude (11 km) flights, Case 4 suggests a 4 $\mu Sv\,h^{-1}$ dose rate at similar altitude midlatitude CONUS regions, and Case 3 suggests a 2 $\mu Sv\,h^{-1}$ dose rate at business jet altitudes (14 km) or a 1 $\mu Sv\,h^{-1}$ dose rate at commercial altitudes (11 km) in equatorial regions. *When there is a minor radiation event*, Case 1 provides an estimate of the ambient dose equivalent rate increasing from 4 to 12 $\mu Sv\,h^{-1}$ (comparable to NAIRAS) between 50° and 40° magnetic midlatitudes and suggests that higher dose rates may occur during larger radiation storms. Although ARMAS has gathered data over 3 years (2013–2016), we do not attempt to study here solar cycle effects on dose rates since Solar Cycle 24 is an abnormally low cycle and the range of variation would be limited in our data.

5.4. Summary Lessons

We can make comparisons between the exposure received in the aviation environment with other radiation sources. If we consider, for example, that a radiography chest X-ray = 100 μSv (0.1 mSv), we note that *with no space weather activity* high-latitude flights (>60°) will produce a minimum dose analogous to a chest X-ray every 12.5 h (100/8), every 25 h for CONUS midlatitudes (100/4), and every 100 h for equatorial latitudes at a typical commercial flight altitude of 37,000 ft (~11 km) (100/1).

If one considers altitude as a variable, we can estimate its effect on dose rate using the Case 1 flight. The DC-8 traversed a nearly constant magnetic longitude with decreasing magnetic midlatitudes on its Winnipeg to Houston leg. Meanwhile, the plane rose and descended between approximately 11 and 13 km. The ambient dose equivalent rate more than doubled from 4.5 $\mu Sv\,h^{-1}$ at 11.0 km to a peak of 11.6 $\mu Sv\,h^{-1}$ at 12.9 km with a rise of 1.9 km (6200 ft) altitude, i.e., a ratio of 2.6. A fraction of this effect may possibly be attributed to the recovering minor *Dst* event (−44 nT) combined with a slight change in magnetic latitude, so we conservatively consider that the dose rate doubles every 2 km or 6200 ft increase in altitude.

5.5. Operational Implications

The combination of these factors implies that one cost-effective radiation event management strategy would be to find lower altitudes or more equatorward flight paths in order to avoid higher radiation regions during events. The task would become one of monitoring, reporting, and identifying event-driven radiation regions to treat them like volcanic ash clouds in aviation operations. In these cases, air traffic control would change the flight routes slightly to lower altitudes or more equatorward flight paths to maintain both radiation safety goals and efficient transportation corridors. Additional work by policy, operational, and scientific stakeholders is needed to set reasonable operational thresholds and response guidelines for enhanced radiation regions.

Acknowledgments

The authors thank the reviewers for their timely and insightful comments that have improved this paper. The authors acknowledge the financial support for ARMAS from the original NASA NAIRAS DECISION project contract NNL07AA00C, the NASA SBIR Phase I and Phase II program contracts NNX11CH03P and NNX12CA78C, the NASA AFRC Phase III contracts NND14SA64P and NND15SA55C, and the South Korean Space Weather Center matching funds for SBIR Phase IIE. Gracious flight support for ARMAS instruments has been provided by the NASA Airborne Sciences Program and Armstrong Flight Research Center. The NOAA Space Weather Prediction Center facilitated use of the NOAA Gulfstream IV through their good offices as did the National Center for Atmospheric Research High Altitude Observatory for the use of the National Science Foundation Gulfstream V. In accordance with the AGU data policy, the ARMAS archival data used in this paper, as well as from all flights, is publically available from the ARMAS website at http://sol.spacenvironment.net/~ARMAS/Level_2_3_Data.html.

References

Beck, P., P. Ambrosi, U. Schrewe, and K. O'Brien (1999), ACREM, aircrew radiation exposure monitoring, Final report of European Commission contract F14P-CT960047, OEFZS, Rep. G-0008.

Beck, P., M. Latocha, S. Rollet, and G. Stehno (2005), TEPC reference measurements at aircraft altitudes during a solar storm, *Adv. Space Res.*, *36*(9), 1627–1633.

Beck, P., C. Dyer, N. Fuller, A. Hands, M. Latocha, S. Rollet, and F. Spurny (2009), Overview of on-board measurements during solar storm periods, *Radiat. Prot. Dosim.*, *136*(4), 297–303, doi:10.1093/rpd/ncp208.

Burda, O., T. Sato, and F. Wissmann (2013), Quality factor of secondary cosmic radiation at flight altitudes, *J. Radiol. Prot.*, *33*(2), 339–348, doi:10.1088/0952-4746/33/2/339.

Cannon, P. (2013), *Extreme Space Weather: Impacts on Engineered Systems and Infrastructure*, Royal Academy of Engineering, London.

Dyer, C., A. Hands, L. Fan, P. Truscott, K. A. Ryden, P. Morris, I. Getley, L. Bennett, B. Bennett, and B. Lewis (2009), Advances in measuring and modeling the atmospheric radiation environment, *IEEE Trans. Nucl. Sci.*, *6*(1), 3415–3422.

Dyer, C. S., A. J. Sims, J. Farren, and J. Stephen (1990), Measurements of solar flare enhancements to the single event upset environment in the upper atmosphere, *IEEE Trans. Nucl. Sci.*, *37*, 1929–1937, doi:10.1109/23.101211.

Executive Order 13744 (2016), The White House, Executive Order—Coordinating efforts to prepare the nation for space weather events, October 13, 2016.

European Commission Radiation Protection 140 (2004), Cosmic radiation exposure of aircraft crew, Compilation of measured and calculated data, European communities.

Gersey, B., R. Wilkins, H. Huff, R. C. Dwivedi, B. Takala, J. O'Donnell, S. A. Wender, and R. C. Singleterry Jr. (2003), Correlation of neutron dosimetry using a silicon equivalent proportional counter microdosimeter and SRAM SEU cross sections for eight neutron energy spectra, *IEEE Trans. Nucl. Sci.*, *50*(6), 2363–2366.

Gersey, B., R. Wilkins, W. Atwell, W. K. Tobiska, and C. Mertens (2012), Tissue equivalent proportional counter microdosimetry measurements aboard high-altitude and commercial aircraft, AIAA 2012–3636, AIAA 42nd International Conference on Environmental Systems, San Diego, Calif., 15–19 July.

Getley, I. L., M. L. Duldig, D. F. Smart, and M. A. Shea (2005), Radiation dose along North American transcontinental flight paths during quiescent and disturbed geomagnetic conditions, *Space Weather*, *3*, S01004, doi:10.1029/2004SW000110.

Getley, I. L., L. G. I. Bennett, B. J. Lewis, B. Bennett, C. S. Dyer, A. D. P. Hands, and M. L. Duldig (2010), Evaluation of new cosmic radiation monitors designed for aircrew exposure assessment, *Space Weather*, *8*, S01001, doi:10.1029/2009SW000492.

Hands, A., and C. S. Dyer (2009), A technique for measuring dose equivalent and neutron fluxes in radiation environments using silicon diodes, *IEEE Trans. Nucl. Sci.*, *56*(1), 3442–3449.

Hubiak, M. (2008), Experimentelle Bestimmung von Dosisraten auf Reiseflughoehen im solaren Minimum, Fachhochschule Muenster University of Applied Sciences, Diploma- Thesis.

ICRU (2011), Reference data for the validation of doses from cosmic-radiation exposure of aircraft crew, Journal of the ICRU, ICRU Report 84, *Radiat. Prot. Dosim.*, doi:10.1093/rpd/ncr110.

International Agency for Research on Cancer (2000), *Ionizing Radiation, Part 1, X- and γ-Radiation and Neutrons*, *IARC Work. Group Eval. Carcinog. Risks Hum.*, vol. 75, IARC and World Health Organization, Lyon, France.

Jones, J. B. L., R. D. Bentley, R. Hunter, R. H. A. Iles, G. C. Taylor, and D. J. Thomas (2005), Space weather and commercial airlines, *Adv. Space Res.*, *36*, 2258–2267.

Kyllönen, J. E., L. Lindborg, and G. Samuelson (2001), Cosmic radiation measurements on board aircraft with the variance method, *Radiat. Prot. Dosim.*, *93*, 197–205.

Latocha, M., M. Autischer, P. Beck, J. F. Bottolier-Depois, S. Rollet, and F. Trompier (2007), The results of cosmic radiation in-flight TEPC measurements during the CAATER flight campaign and comparison with simulation, *Radiat. Prot. Dosim.*, *125*(1–4), 412–415, doi:10.1093/rpd/ncl123.

Lee, J., U.-W. Nam, J. Pyo, S. Kim, Y.-J. Kwon, J. Lee, I. Park, M.-H. Y. Kim, and T. P. Dachev (2015), Short-term variation of cosmic radiation measured by aircraft under constant flight conditions, *Space Weather*, *13*, 797–806, doi:10.1002/2015SW001288.

Mazur, J. E., W. R. Crain, M. D. Looper, D. J. Mabry, J. B. Blake, A. W. Case, M. J. Golightly, J. C. Kasper, and H. E. Spence (2011), New measurements of total ionizing dose in the lunar environment, *Space Weather*, *9*, S07002, doi:10.1029/2010SW000641.

Meier, M. M., M. Hubiak, D. Matthiä, M. Wirtz, and G. Reitz (2009), Dosimetry at aviation altitudes (2006–2008), *Radiat. Prot. Dosim.*, *136*(4), 251–255.

Meier, M. M., D. Matthiä, T. Forkert, M. Wirtz, M. Scheibinger, R. Hübel, and C. J. Mertens (2016), RaD-X: Complementary measurements of dose rates at aviation altitudes, *Space Weather*, *14*, 689–694, doi:10.1002/2016SW001418.

Mertens, C. J., B. T. Kress, M. Wiltberger, S. Blattnig, T. S. Slaba, S. C. Solomon, and M. Engel (2010), Geomagnetic influence on aircraft radiation exposure during a solar energetic particle event in October 2003, *Space Weather*, *8*, S03006, doi:10.1029/2009SW000487.

Mertens, C. J., B. T. Kress, M. Wiltberger, W. K. Tobiska, B. Grajewski, and X. Xu (2012), Atmospheric ionizing radiation from galactic and solar cosmic rays, in *Current Topics in Ionizing Radiation Research*, edited by M. Nenoi, pp 683–738, InTech, ISBN: 978-953-51-0196-3. [Available from: http://www.intechopen.com/books/current-topics-in-ionizing-radiation-research/atmospheric-ionizing-radiationfrom-galactic-and-solar-cosmic-rays.]

Mertens, C. J., M. M. Meier, S. Brown, R. B. Norman, and X. Xu (2013), NAIRAS aircraft radiation model development, dose climatology, and initial validation, *Space Weather*, *11*, 603–635, doi:10.1002/swe.20100.

Mertens, C. J., et al. (2016), Cosmic radiation dose measurements from the RaD-X flight campaign, *Space Weather*, *14*, doi:10.1002/2016SW001407.

National Science and Technology Council (2015), National Space Weather Action Plan, October 2015.

Ploc, O., I. Ambrozova, J. Kubancak, I. Kovar, and T. P. Dachev (2013), Publicly available database of measurements with the silicon spectrometer Liulin onboard aircraft, *Radiat. Meas.*, *58*, 107–112.

Schwadron, N. A., et al. (2012), Lunar radiation environment and space weathering from the Cosmic Ray Telescope for the Effects of Radiation (CRaTER), *J. Geophys. Res.*, *117*, E00H13, doi:10.1029/2011JE003978.

Straume, T., C. J. Mertens, T. C. Lusby, B. Gersey, W. K. Tobiska, R. B. Norman, G. P. Gronoff, and A. Hands (2016), Ground-based evaluation of dosimeters for NASA high-altitude balloon flight, *Space Weather*, *14*, doi:10.1002/2016SW001406.

Tobiska, W. K., B. Gersey, R. Wilkins, C. Mertens, W. Atwell, and J. Bailey (2014a), U.S. Government shutdown degrades aviation radiation monitoring during solar radiation storm, *Space Weather*, *12*, 41–45, doi:10.1002/2013SW001015.

Tobiska, W. K., B. Gersey, R. Wilkins, C. Mertens, W. Atwell, and J. Bailey (2014b), Reply to comment by Rainer Facius et al. on "U.S. Government shutdown degrades aviation radiation monitoring during solar radiation storm", *Space Weather*, *12*, 320–321, doi:10.1002/2014SW001074.

Tobiska, W. K., et al. (2015), Advances in atmospheric radiation measurements and modeling needed to improve air safety, *Space Weather*, *13*, 202–210, doi:10.1002/2015SW001169.

United Nations Scientific Committee on the Effect of Atomic Radiation (2000), Sources and effect of ionizing radiation, United Nations Scientific Committee on the Effect of Atomic Radiation UNSCEAR 2000 Report to the General Assembly, with Scientific Annexes, Vol. II, Annex G.

Wilson, J. W., J. E. Nealy, F. A. Cucinotta, J. L. Shinn, F. Hajnal, M. Reginatto, and P. Goldhagen (1995), Radiation safety aspects of commercial high-speed flight transportation, NASA Tech. Pap. 3524.